



- (51) **International Patent Classification:**
A61F 2/02 (2006.01)
- (21) **International Application Number:**
PCT/US20 15/060329
- (22) **International Filing Date:**
12 November 2015 (12.11.2015)
- (25) **Filing Language:** English
- (26) **Publication Language:** English
- (30) **Priority Data:**
62/080,082 14 November 2014 (14.11.2014) US
- (71) **Applicant:** THE UNIVERSITY OF FLORIDA RESEARCH FOUNDATION, INC. [US/US]; 233 Grinter Hall, Gainesville, FL 32611 (US).
- (72) **Inventors:** HARDY, John; 4 Warding Drive, Little Common Bexhill-on-sea, East Sussex TN39 4QN (GB). SCHMIDT, Christine, E.; 1922 Sw 106th Terrace, Gainesville, FL 32607 (US).
- (74) **Agents:** LINDER, Christopher, B. et al; Thomas / Horstemeyer LLP, 400 Interstate North Parkway, Se, Suite 1500, Atlanta, GA 30339 (US).
- (81) **Designated States** (unless otherwise indicated, for every kind of national protection available): AE, AG, AL, AM, AO, AT, AU, AZ, BA, BB, BG, BH, BN, BR, BW, BY, BZ, CA, CH, CL, CN, CO, CR, CU, CZ, DE, DK, DM,

DO, DZ, EC, EE, EG, ES, FI, GB, GD, GE, GH, GM, GT, HN, HR, HU, ID, IL, IN, IR, IS, JP, KE, KG, KN, KP, KR, KZ, LA, LC, LK, LR, LS, LU, LY, MA, MD, ME, MG, MK, MN, MW, MX, MY, MZ, NA, NG, NI, NO, NZ, OM, PA, PE, PG, PH, PL, PT, QA, RO, RS, RU, RW, SA, SC, SD, SE, SG, SK, SL, SM, ST, SV, SY, TH, TJ, TM, TN, TR, TT, TZ, UA, UG, US, UZ, VC, VN, ZA, ZM, ZW.

(84) **Designated States** (unless otherwise indicated, for every kind of regional protection available): ARIPO (BW, GH, GM, KE, LR, LS, MW, MZ, NA, RW, SD, SL, ST, SZ, TZ, UG, ZM, ZW), Eurasian (AM, AZ, BY, KG, KZ, RU, TJ, TM), European (AL, AT, BE, BG, CH, CY, CZ, DE, DK, EE, ES, FI, FR, GB, GR, HR, HU, IE, IS, IT, LT, LU, LV, MC, MK, MT, NL, NO, PL, PT, RO, RS, SE, SI, SK, SM, TR), OAPI (BF, BJ, CF, CG, CI, CM, GA, GN, GQ, GW, KM, ML, MR, NE, SN, TD, TG).

Declarations under Rule 4.17:

- as to applicant's entitlement to apply for and be granted a patent (Rule 4.17(H))
- as to the applicant's entitlement to claim the priority of the earlier application (Rule 4.17(in))
- of inventorship (Rule 4.17(iv))

Published:

- with international search report (Art. 21(3))

(54) **Title:** BIOMIMETIC PORE STRUCTURES AND METHODS OF MAKING BIOMIMETIC PORE STRUCTURES

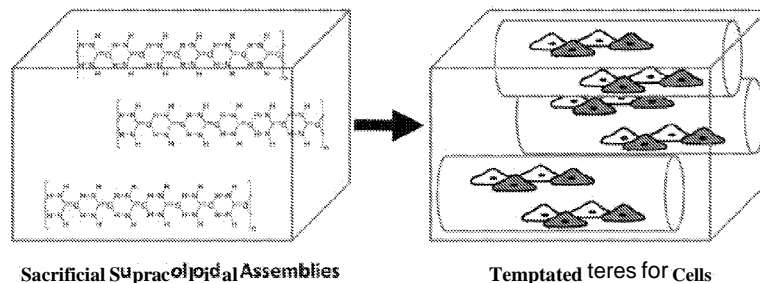


Fig. 1.1

(57) **Abstract:** Embodiments of the present disclosure provide for tissue scaffolds, biodegradable porous tissue scaffolds, biodegradable electroactive tissue scaffolds, biodegradable electroactive porous tissue scaffolds, methods of making each type of tissue scaffold, methods of using each type of tissue scaffold, and the like.

WO 2016/077551 A1

BIOMIMETIC PORE STRUCTURES AND METHODS OF MAKING BIOMIMETIC PORE STRUCTURES

CROSS-REFERENCE TO RELATED APPLICATIONS

This application claims the benefit of and priority to U.S. Provisional Application Serial No. 62/080,082, having the title "Urea-Templated Materials," filed on November 14, 2014, the disclosure of which is incorporated herein in by reference in its entirety.

STATEMENT REGARDING FEDERALLY SPONSORED RESEARCH OR DEVELOPMENT

This invention was made with Government support under contract DMR 0805298 awarded by the National Science Foundation. The Government has certain rights in the invention.

BACKGROUND

Tissues in the body are hierarchically structured composite materials with tissue-specific properties. Although it is possible to employ 3D printing technologies to prepare porous materials, it is challenging to fabricate porous structures accurately mimicking native tissues. Thus, there is a need to overcome difficulties in known methods or find alternatives.

SUMMARY

Embodiments of the present disclosure provide for tissue scaffolds, biodegradable porous tissue scaffolds, biodegradable electroactive tissue scaffolds, biodegradable electroactive porous tissue scaffolds, methods of makes each type of tissue scaffold, methods of using each type of tissue scaffold, and the like.

An embodiment of the present disclosure provides for a method of forming a tissue scaffold, among others, that includes: mixing a solution including urea and a non-aqueous solvent with a polymer that is soluble with the solvent to form a mixture; disposing the mixture on a substrate; and removing the solvent from the mixture to form a tissue scaffold. In an embodiment, the method can also include: removing the urea from the tissue scaffold to form a biodegradable porous tissue scaffold, wherein removal of the urea forms pores within the tissue scaffold to form the biodegradable porous tissue scaffold. In an embodiment, the

non-aqueous solvent can be: formic acid, trifluoroacetic acid, hexafluoroisopropanol, hexafluoroacetone hydrate, methanol, ethanol, propanol, isopropanol, acetophenone, methoxyethanol, ethanediol, 1,2-propanediol, 1,3-propanediol, glycerol, glycerol monoacetate, glycerol diacetate, methylacetate, ethylacetate, allyl alcohol, furfuryl alcohol, diacetone alcohol, benzyl alcohol, cyclohexanol or a combination thereof. In an embodiment, the polymer is selected from the group consisting of: nylon, hydroxybutyric acids, polyanhydrides, polphosphazenes, polyphosphoesters, polyethers, polysilanes, polysiloxanes, polyurethanes,) polycaprolactone, polyesters, polyamides, PCL, PLLA, PLGA, lignins, polyalanine, oligoalanine, collagen, silk, cellulose, chitin, chitosan, dextran, or a combination thereof.

In an embodiment, the method can include an electroactive tissue scaffold by polymerizing an electroactive polymer with the tissue scaffold. In an embodiment, the method can include removing the urea from the electroactive tissue scaffold to form a biodegradable electroactive porous tissue scaffold, wherein removal of the urea forms pores within the tissue scaffold to form the biodegradable electroactive porous tissue scaffold. In an embodiment, the electroactive polymer can be: polypyrrole, polyaniline, polythiophene, poly(3,4-ethylenedioxythiophene), poly fluorenes, polyphenylenes, polypyrenes, polyazulenes, polynaphthalenes, polyindoles, polyazepines, poly(p-phenylene sulfide)s, poly(p-phenylene vinylene)s, polyfurans, or a combination thereof.

In an embodiment, the substrate can includes a network of channels, wherein the mixture is disposed in the network of channels, wherein the method further includes: removing the substrate to form the tissue scaffold having a network of pores extending through the tissue scaffold. The network of channels are aligned relative to one another and each of the channels in the network of channels has a diameter of about 50 nm to 100 μm and the length of about 1 cm to 10 cm. In an embodiment, the method also includes removing the urea from the tissue scaffold to form a biodegradable porous tissue scaffold, wherein removal of the urea forms pores within the tissue scaffold to form the biodegradable porous tissue scaffold.

In an embodiment, the pores formed from removal of the urea are of the type selected from the group consisting of: dendritic, linear, and a combination thereof.

An embodiment of the present disclosure includes a structure, among others, that includes: a tissue scaffold including a polymer and urea, wherein the polymer is soluble in a non-aqueous solvent selected from the group consisting of: formic acid, trifluoroacetic acid, hexafluoroisopropanol, hexafluoroacetone hydrate, methanol, ethanol, propanol, isopropanol,

acetophenone, methoxyethanol, ethanediol, 1,2-propanediol, 1,3-propanediol, glycerol, glycerol monoacetate, glycerol diacetate, methylacetate, ethylacetate, allyl alcohol, furfuryl alcohol, diacetone alcohol, benzyl alcohol, cyclohexanol and a combination thereof. In addition, the structure can include an electroactive polymer. The urea is in the form of urea crystals, wherein the urea crystals have a crystal structure selected from the group consisting of: dendritic, linear, or a combination thereof.

BRIEF DESCRIPTION OF THE DRAWINGS

Many aspects of the present disclosure can be better understood with reference to the following drawings.

Figure 1.1 demonstrates hydrogen bond mediated self-assembly of supracolloidal assemblies of urea that act as sacrificial templates to impart pores in biomaterials.

Figures 1.2A-D are brightfield microscope images of urea crystals. (1.2A) Formed by uncontrolled crystallization from solutions of urea in formic acid (scale bar, 200 μm); (1.2B) Formed by uncontrolled crystallization from solutions of urea in hexafluoroacetone hydrate (scale bar, 200 μm); (1.2C) Formed by uncontrolled crystallization from solutions of urea in hexafluoroisopropanol (scale bar, 200 μm); and (1.2D) Formed by controlled crystallization from solutions of urea in hexafluoroisopropanol in a Pasteur pipette (scale bar, 500 μm).

Figures 1.3A-F are images of urea crystal-templated silk films. (1.3A) Brightfield microscope image of urea crystal-templated silk films from solution in formic acid (scale bar, 600 μm); (1.3B) SEM image of urea crystal-templated silk films formed from solution in formic acid (scale bar, 200 μm); (1.3C) Brightfield microscope image of urea crystal-templated silk films formed from solution in hexafluoroacetone hydrate (scale bar, 600 μm); (1.3D) SEM image of urea crystal-templated silk films formed from solution in hexafluoroacetone hydrate (scale bar, 100 μm); (1.3E) SEM image of urea crystal-templated silk films formed from solution in hexafluoroisopropanol (scale bar, 100 μm); and (1.3F) SEM image of urea crystal-templated silk films formed from solution in water (scale bar, 100 μm). Images are representative of at least 3 locations on 3 samples.

Figure 1.4 is an image of fibroblasts on the surface of the porous silk substrates stained with DAPI (nuclei) and Alexa Fluor 488[®] Phalloidin (actin filaments); scale bar, 100 μm . Images are representative of at least 3 locations on 3 samples.

Figure 2.1 is a hydrogen bond-mediated self-assembly of urea.

Figures 2.2A-D demonstrate the template manufacture process. (2.2A) Illustration of the experimental setup used to produce the hard acrylic master template with grooves with

widths and heights of 2 mm. (2.2B) Examples of the hard acrylic master templates produced: (left) grooves with widths and heights of 2 mm; (center) grooves with widths and heights of 1 mm; (right) grooves with widths and heights of 0.5 mm. (2.2C) Examples of the flexible PDMS templates produced: (left) grooves with widths and heights of 2 mm; (right) grooves with widths and heights of 1 mm. (2.2D) Illustration of the experimental setup using the flexible, grooved PDMS template covered with a glass slide, which facilitates controlled solvent evaporation and thereby preferential alignment of urea crystals within the grooves.

Figure 2.3 is an experimental setup for electrical stimulation of electroactive PCL-based tissue scaffolds (not to scale). (CE) counter electrode. (CT) copper tape. (PCL) electroactive PCL-based tissue scaffolds. (PCW) polycarbonate well. (RE) reference electrode. (WE) working electrode.

Figures 2.4A-D are scanning electron microscope images of sections of PCL-based tissue scaffolds with aligned pores. (2.4A) Millimeter and micrometer scale topography of non-electroactive scaffolds, scale bar represents 500 μm . (2.4B) Micrometer and nanometer scale topography of non-electroactive scaffolds, scale bar represents 10 μm . (2.4C) Millimeter and micrometer scale topography of electroactive scaffolds, scale bar represents 500 μm . (2.4D) Micrometer and nanometer scale topography of electroactive scaffolds showing evidence of increased nanometer scale surface roughness due to the presence of an interpenetrating network of PPy and PSS interwoven within the PCL matrix, scale bar represents 10 μm .

Figures 2.5A-D demonstrates spectroscopic analysis of PCL-based tissue scaffolds. (2.5A and 2.5B) FTIR spectra of PCL-based tissue scaffolds with aligned pores: (2.5A) non-electroactive scaffolds, (2.5B) electroactive scaffolds. Peaks observed at ca. 1543 and ca. 1480 cm^{-1} are characteristic of the antisymmetric and symmetric ring stretching modes of pyrrole [65,78]. (C and D) XPS spectra of PCL-based tissue scaffolds with aligned pores: (2.5C) non-electroactive scaffolds, (2.5D) electroactive scaffolds. Peaks at ca. 400 eV (N 1s) and ca. 168 eV (S 2p) are characteristic of PPy and PSS, respectively [65,79].

Figure 2.6A-B are *in vitro* degradation profiles of the PCL-based tissue scaffolds in PBS. (2.6A) Non-electroactive scaffolds: black circles in the absence of cholesterol esterase; grey circles in the presence of cholesterol esterase. (2.6B) Electroactive scaffolds: black circles in the absence of cholesterol esterase; grey circles in the presence of cholesterol esterase. Error bars represent standard deviations.

Figures 2.7A-B show that cells respond to the topography of the PCL-based tissue scaffolds substrates and align on the substrates. (2.7A) Schwann cells on non-electroactive

scaffolds (scale bar represents 50 μm); (2.7B) Schwann cells on electroactive scaffolds without electrical stimulation (scale bar represents 50 μm).

Figure 2.8 graphs the concentration of Schwann cell-produced NGF in the culture medium. Black circles) commercially available tissue-culture treated Corning® Costar® tissue culture plates. (Red circles) non-electroactive PCL-based tissue scaffolds. (Yellow circles) electroactive PCL-based tissue scaffolds without electrical stimulation. (Blue circles) electroactive PCL-based tissue scaffolds with electrical stimulation. Error bars represent standard deviations.

DETAILED DESCRIPTION

This disclosure is not limited to particular embodiments described, and as such may, of course, vary. The terminology used herein serves the purpose of describing particular embodiments only, and is not intended to be limiting, since the scope of the present disclosure will be limited only by the appended claims.

Where a range of values is provided, each intervening value, to the tenth of the unit of the lower limit unless the context clearly dictates otherwise, between the upper and lower limit of that range and any other stated or intervening value in that stated range, is encompassed within the disclosure. The upper and lower limits of these smaller ranges may independently be included in the smaller ranges and are also encompassed within the disclosure, subject to any specifically excluded limit in the stated range. Where the stated range includes one or both of the limits, ranges excluding either or both of those included limits are also included in the disclosure.

As will be apparent to those of skill in the art upon reading this disclosure, each of the individual embodiments described and illustrated herein has discrete components and features which may be readily separated from or combined with the features of any of the other several embodiments without departing from the scope or spirit of the present disclosure. Any recited method may be carried out in the order of events recited or in any other order that is logically possible.

Embodiments of the present disclosure will employ, unless otherwise indicated, techniques of organic chemistry, biochemistry, microbiology, molecular biology, pharmacology, medicine, and the like, which are within the skill of the art. Such techniques are explained fully in the literature.

Prior to describing the various embodiments, the following definitions are provided and should be used unless otherwise indicated.

Unless otherwise defined, all technical and scientific terms used herein have the same meaning as commonly understood by one of ordinary skill in the art of microbiology, molecular biology, medicinal chemistry, and/or organic chemistry. Although methods and materials similar or equivalent to those described herein can be used in the practice or testing of the present disclosure, suitable methods and materials are described herein.

As used in the specification and the appended claims, the singular forms "a," "an," and "the" may include plural referents unless the context clearly dictates otherwise. Thus, for example, reference to "a support" includes a plurality of supports. In this specification and in the claims that follow, reference will be made to a number of terms that shall be defined to have the following meanings unless a contrary intention is apparent.

Discussion:

Embodiments of the present disclosure provide for tissue scaffolds, biodegradable porous tissue scaffolds, biodegradable electroactive tissue scaffolds, biodegradable electroactive porous tissue scaffolds, methods of making each type of tissue scaffold, methods of using each type of tissue scaffold, and the like.

In an embodiment of the present disclosure a sacrificial biodegradable material (*e.g.*, urea crystals) can be removed from a tissue scaffold to form a porous tissue scaffold. Removal of sacrificial material from a matrix is a comparatively low cost alternative that allows the generation of hierarchically organized pores in the tissue scaffold. Selection of non-aqueous solvents can be used to expand the scope of polymers that are compatible with, while selection of non-aqueous solvents in conjunction with specific polymers allow control of the topography (*e.g.*, type (*e.g.*, linear, dendritic, or a combination thereof) and dimensions (*e.g.*, on the nanoscale) of the pores) of the tissue scaffold. Embodiments of the present disclosure discuss the role of solvent interactions on the morphology of the resulting supracolloidal crystals. In particular, embodiments of the present disclosure can be used to prepare silk (*e.g.*, *B. mori* silk) protein-based biomaterials with pores that cells (*e.g.*, human dermal fibroblasts, Schwann cells, and the like) respond to by aligning with the long axis of a network of macroscale pores. Embodiments of the present disclosure can be used in tissue engineering in which cell alignment is observed, including skin, bone, muscle and nerve. Additional details are provided herein and in the Examples.

In an embodiment, the tissue scaffolds can be made so that they also have electroactive properties that can allow for electrical stimulation of, for example, cells cultured on the tissue scaffolds. The electrical stimulation can be applied periodically. In a particular

embodiment, a cell and/or tissue can be incubated with the electroactive tissue scaffold and cultured in an appropriate medium so that the cells are stimulated. In an embodiment, the electrical stimulation increased the production of nerve growth factor (NGF) to more than three times the amount produced by non-stimulated cells, which may improve clinical outcomes during peripheral nerve regeneration. Additional details are provided herein and in the Examples.

In an embodiment, tissue scaffolds of the present disclosure can be used to deliver agents such as drugs, antibacterial agents, and antifungal agents.

An embodiment of the present disclosure includes forming a tissue scaffold. In an embodiment, the method includes mixing a solution including urea (*i.e.*, $\text{CO}(\text{NH}_2)_2$) and a non-aqueous solvent with a polymer that is soluble with the solvent to form a mixture. The ratio of the amount of polymer to urea can be about 99 to 1 or about 1 to 4. The mixture is disposed on a substrate and then the solvent is removed from the mixture in a controlled or uncontrolled manner. Uncontrolled evaporation of the solvent typically results in crystals not being aligned, whereas, by controlling evaporation such that solvent preferentially evaporates from one or more specific positions it is possible to initiate the crystallization of urea to yield long, directionally aligned crystals. The urea crystals formed can be of the dendritic type, linear type, or a combination thereof. The type and dimensions (*e.g.*, nanoscale (*e.g.*, about 50 nm to 500 μm) or about 1 to 500 μm) of the urea crystals formed can be controlled by selection of the non-aqueous solvent and the polymer.

Subsequently, the urea crystals can be removed from the tissue scaffold to form a biodegradable porous tissue scaffold. Removing the urea crystals forms pores within the tissue scaffold, where the pores have nanoscale dimensions and are separate from the network of pores described shortly which are of the microscale. The pores formed from removal of the urea crystals are of the types: dendritic, linear, and a combination thereof. Additional details are described in the Examples.

In an embodiment, the polymer is insoluble or sparingly soluble ($<0.1 \text{ mg ml}^{-1}$) in water. The polymer is soluble in a non-aqueous solvent such as formic acid, trifluoroacetic acid, hexafluoroisopropanol, hexafluoroacetone hydrate, methanol, ethanol, propanol, isopropanol, acetophenone, methoxyethanol, ethanediol, 1,2-propanediol, 1,3-propanediol, glycerol, glycerol monoacetate, glycerol diacetate, methylacetate, ethylacetate, allyl alcohol, furfuryl alcohol, diacetone alcohol, benzyl alcohol, cyclohexanol and a combination thereof.

The polymer can include a synthetic polymer (*e.g.*, polyesters, polyamides, polyurethanes, PCL, PLLA, PLGA, nylon, hydroxybutyric acids, polyanhydrides,

polphosphazenes, polyphosphoesters, polyethers, polysilanes, polysiloxanes or pellethane), a natural polymer (*e.g.* proteins, polysaccharides, lignins, polyalanine, oligoalanine, collagen, silk, cellulose, chitin, chitosan, or dextran), or a combination thereof. In an embodiment, the tissue scaffold can include a mixture of different types of polymers (*e.g.*, a portion of polycaprolactone polymer and another polyester).

In an embodiment, an electroactive polymer can be included in the tissue scaffold. In an embodiment the electroactive polymer can be added to the tissue scaffold after the polymer is mixed with the urea to form the tissue scaffold or the electroactive polymer, polymer, and urea can be mixed together prior to forming the tissue scaffold. Introduction of the electroactive polymer to the tissue scaffold can produce an electroactive tissue scaffold and removal of the urea can result in the formation of an electroactive porous tissue scaffold.

In this regard, embodiments of the present disclosure include tissue scaffolds (*e.g.*, biodegradable electroactive tissue scaffolds, biodegradable electroactive porous tissue scaffolds) that include a polymerizable electrically responsive unit (*e.g.*, pyrrole) that is attached by polymerization (*e.g.*, covalently, non-covalently, or as an interpenetrating network) within the polymer matrix (*e.g.*, polycaprolactone matrix) in order to form an electroactive tissue scaffold upon which cells or tissues can be cultured. In an embodiment, the micro- and nano-topological features (*e.g.*, grooves, pores, bumps or other topological features) of the matrix can be preserved during polymerization with the unit. In an embodiment, electroactive tissue scaffolds can also be used as electroactive actuators capable of mechanotransduction of cells such as stem cells.

In an embodiment, the electroactive polymer (conducting polymer) can include polymers such as polypyrrole, polyaniline, polythiophene, poly(3,4-ethylenedioxythiophene), poly fluorenes, polyphenylenes, polypyrenes, polyazulenes, polynaphthalenes, polyindoles, polyazepines, poly(p-phenylene sulfide)s, poly(p-phenylene vinylene)s, and polyfurans. In an embodiment, there are biodegradable versions, in which there are block of conducting units within a polymer chain containing biodegradable bonds (*e.g.* esters and amides), that can also be used as the conducting polymer. In an embodiment, the electroactive polymer can be used in conjunction with a dopant. The dopant can be a polymer that has the opposite charge to the conducting polymer, and can be low molecular weight (*e.g.*, chlorine ions, tosylate ions, and the like) or high molecular weight (*e.g.*, collagen, hyaluronic acid, and the like).

In an embodiment, the electroactive polymer can be about 1 to 99 or about 2 to 10 weight percent of the tissue scaffold.

As mentioned above, the mixture is disposed on a substrate. In an embodiment, the substrate can be flat or can have contours (*e.g.*, to form topographic features in or through the tissue scaffold). In an embodiment, the substrate can be used to form a network of pores or channels that extend through the width of the tissue scaffold. In addition the network of channels can be aligned relative to one another, which can be achieved by controlled evaporation of the solvent from the mixture (polymer/urea solution), thereby initiating directional crystallization of the urea. In an embodiment, the substrate can include a network of channels and areas outside of the network of channels. The mixture can be disposed in the network of channels but not on the areas outside of the network of channels. The mixture can be dried and the tissue scaffold formed according to the topography of the substrate so that a network of pores extends through the tissue scaffold. In an embodiment, each of the pores in the network of pores has a diameter, if spherical, or other dimension if not spherical, of about 10 nm to 500 μm or about 50 nm to 100 μm and has a length through the tissue scaffold (or the width of the tissue scaffold) of about 1 cm to 10 cm or about 0.5 cm to 3 cm. In an embodiment, the tissue scaffold has pore as a result of the structure and as a result of the removal of the urea crystals.

Having described embodiments of making tissue scaffolds, additional details regarding tissue scaffolds are now described. As mentioned above, various types of tissue scaffolds have been disclosed including: biodegradable porous tissue scaffolds, biodegradable electroactive tissue scaffolds, biodegradable electroactive porous tissue scaffolds, and the like. The term "biodegradable" refers to polymers that degrade through the action of a physicochemical (*e.g.*, hydrolysis, pH) or biological (*e.g.*, enzyme) trigger that the polymer is exposed to in use.

An embodiment of the tissue scaffold includes a tissue scaffold including the polymer and urea, wherein the polymer is not soluble in water. In this embodiment the urea has not yet been removed. Once the urea is removed, the tissue scaffold can be porous due to the removal of the urea crystals. In this regard, the type and/or dimension of the urea crystals that are formed can be controlled so that pores formed upon their removal have a certain porous structure (*e.g.*, dendritic, linear). In an embodiment, the tissue scaffold can include an electroactive polymer to produce an electroactive tissue scaffold. In addition, the topography of the tissue scaffold can be tailored to accomplish desired goals. For example, the topography can be tailored using the substrate, where in an embodiment, the substrate is designed so that a network of channels is formed through the tissue scaffold.

As mentioned above, embodiments of the disclosure provide for methods of stimulating cells or tissue. An embodiment of the present disclosure includes introducing cells to the tissue scaffold, where the tissue scaffold (and optionally a tissue or other cells) and the cells are cultured in an appropriate medium. Subsequently, electrical stimulation can be periodically applied to the cells to cause a desired outcome.

Electrical stimulation can include direct contact of the material with a power source via a wire, wireless energy transfer, magnetic force, and the like. The term "periodically" refers to applying the electrical stimulation at established time frames that may be at regular or irregular time intervals on the time frames of seconds, hours, days, weeks, or months (*e.g.*, about 1 s to 2 months, about 1 hour to 1 day, about 1 day to 1 month, or other the like) depending upon the specific circumstances. In an embodiment, the impulses of the electrical stimulation can last on the time frame of seconds, hours, or days (*e.g.*, about 1 second to 1 day, about 10 seconds to 1 hour, about 1 minute to 12 hours, about 1 hour to 1 day, or the like) depending upon the specific circumstances. In an embodiment, the electrical stimulation can be in the range of millivolts to volts (*e.g.*, about 10 mV to 10 volts, about 1 mV to 100 mV, or the like). The time frame, duration of electrical stimulation, and intensity of the electrical stimulation can be designed based on particular circumstances and requirements of a specific situation.

In an embodiment, the tissue scaffold can include one or more agents (*e.g.*, a chemical or biological agent), where the agent can be disposed indirectly or directly on the tissue scaffold. In an embodiment, the agent can include, but is not limited to, a drug, a therapeutic agent, a radiological agent, a small molecule drug, a biological agent (*e.g.*, polypeptides (*e.g.*, proteins such as, but not limited to, antibodies (monoclonal or polyclonal)), antigens, nucleic acids (both monomeric and oligomeric), polysaccharides, haptens, sugars, fatty acids, steroids, purines, pyrimidines, ligands, and aptamers) and combinations thereof, that can be used to image, detect, study, monitor, evaluate, and the like. In an embodiment, the agent is included in an effective amount to accomplish its purpose, where such factors to accomplish the purpose are well known in the medical arts.

In general, the agent can be bound to the tissue scaffold by a physical, biological, biochemical, and/or chemical association directly or indirectly by a suitable means. The term "bound" can include, but is not limited to, chemically bonded (*e.g.*, covalently or ionically), biologically bonded, biochemically bonded, and/or otherwise associated with the material. In an embodiment, being bound can include, but is not limited to, a covalent bond, a non-covalent bond, an ionic bond, a chelated bond, as well as being bound through interactions

such as, but not limited to, hydrophobic interactions, hydrophilic interactions, charge-charge interactions, π - π stacking interactions, combinations thereof, and like interactions."

While embodiments of the present disclosure are described in connection with the Examples and the corresponding text and figures, there is no intent to limit the disclosure to the embodiments in these descriptions. On the contrary, the intent is to cover all alternatives, modifications, and equivalents included within the spirit and scope of embodiments of the present disclosure.

EXAMPLE:

Example 1:

Bodily tissues are hierarchically structured composite materials with tissue-specific properties that act as cues that dictate the behavior of cells that inhabit them, and such properties can potentially be engineered into instructional tissue scaffolds to achieve similar results [1-6]. Topographical control of cell alignment is clearly observable within anisotropically aligned pores that are observed in bone, muscle, nerve and other tissues, which motivates the development of novel methodologies of imparting biomimetic porous structures within biomaterials [1-6].

Silk protein-based materials are produced by a number of different species (the most widely studied being that of the domesticated *B. mori* silkworm) [5,7-10], many of which display interesting mechanical properties and low immunogenicity, and have led to the development of engineered silk-inspired proteins produced recombinantly [11-15], or silk-inspired polymers produced by synthetic chemists [15]. Silk-based biomaterials are popular for a variety of applications because of: (1) their ease of processing in a variety of different solvents (including water, ionic liquids, formic acid, hexafluoroacetone hydrate and hexafluoroisopropanol); (2) the morphologies that can be manufactured (fibers, films, foams, hydrogels); and (3) their ease of chemical modification [7-15]. Silk-based biomaterials and their composites are capable of controlled drug delivery, and of acting as cell adhesive tissue scaffolds for a variety of different niches both *in vitro* and *in vivo* [7-15].

Although it is possible to employ 3D printing technologies to prepare porous materials, it is challenging to fabricate porous structures accurately mimicking native tissues [1-6]. The removal of sacrificial templates (e.g., colloidal crystals, ice crystals, electrospun fibers) from a matrix is an alternative approach that allows the generation of hierarchically organized pores in materials [1-6], potentially on the nanoscale [16]. Urea is an inexpensive, non-toxic solid that self-assembles into supracolloidal crystals. The uncontrolled evaporation

of water from aqueous solutions of urea yields random networks of dendritic crystals, whereas controlled use of urea seed crystals to initiate crystallization yields relatively well aligned crystals over the length scale of a few hundred micrometers [17]. Zawko and coworkers reported the use of urea to impart pores within photocrosslinkable biopolymer-based hydrogels that typically have mechanical properties similar to soft, and fibroblasts cultured within the gels were observed to align parallel to the fibrillar microstructure of the hydrogels [17]. While entirely aqueous manufacturing processes are appealing, they restrict the selection of materials used to those that are soluble in water (e.g., polysaccharides), and there are many water insoluble polymers used in the clinic. Therefore we used a non-aqueous solvent hexafluoroisopropanol (HFIP) to generate urea-templated polycaprolactone foams [18]. We also reported a simple scalable methodology for aligning the supracolloidal crystals that allows the generation of pores that were aligned over length scales of multiple centimeters within which Schwann cells from the peripheral nervous system aligned [18].

In this Example, we explain the solvent interactions governing the solubility of urea which enables us to expand the range of solvents compatible with our urea-based supracolloidal crystal templating methodology, and thereby broadens the scope of polymers it is compatible with. We also highlight the role of solvent interactions on the morphology of the resulting supracolloidal crystals, and moreover, the role of polymer-porogen (silk-urea) interactions on the morphology of the pores in the resulting biomaterials. Finally, we demonstrate that it is possible to use our urea templating methodology to prepare silk protein-based biomaterials with aligned pores that permit cell growth and alignment (Figure 1.1).

Results and Discussion

Urea Solubility in Non-Aqueous Solvents

A parameterized approach was used to investigate the ability of non-aqueous solvents to dissolve urea. Solvent-solute interactions play an important role in supramolecular chemistry which has led to quantitative studies of the role of solvents in self-assembly processes [19-24]. The bulk properties (e.g., boiling point, density) or molecular level properties (such as specific intermolecular forces) can be quantified and parameterized. Bulk property parameters include the dielectric constant (ϵ) and Reichardt's parameter (E_T , a measure of ionizing power). Molecular level parameters include the Hildebrand solubility parameter, δ (expressed in terms of the total solubility parameter, δ_o , which is described by the dispersion, polar, and hydrogen bonding parameters, δ_d , δ_p , and $\delta_{3/4}$ respectively). The parameters δ_p and δ_H are described in terms of a combined polar solubility parameter, δ_a , and

the Kamlet-Taft parameters, π^* (a generalized polarity parameter), α (the ability to donate hydrogen bonds), and β (the ability to accept hydrogen bonds). The effects of solvents on the hierarchical assembly of supramolecular polymers in non-aqueous solvents have been studied for self-assembling peptides, and while there was a general correlation between the ability of supramolecular polymers to form and the polar solubility parameter, δ_a [19-24], the precise hydrogen-bonding nature of the solvent in terms of Kamlet-Taft parameters (*i.e.*, deconvolution of the hydrogen bond donors and acceptors) was important to fully understand the solvent effects [19-24]. Hydrogen bond donor solvents but not acceptors, played a key role in disrupting amide-mediated self-assembly in non-aqueous solvents.

To generate highly porous biomaterials we require the sacrificial template to be highly soluble in the solvent used during polymer processing. Thus we investigated the ability of a variety of non-aqueous solvents to dissolve urea at a concentration of 100 mg/mL (see Table 1.1), an arbitrary concentration equivalent to the concentration of polymer, thereby assuring the presence of pores with micrometer scale diameters in the resulting materials.

Solvent	ϵ	E_T	π^*	α	β	Boiling point (°C)	Surface tension (mN/m)	Solubility of Urea
Cyclohexane	2.10	0.006	0.00	0.00	0.00	80.7	25.0	I.S.
Toluene	2.38	0.099	0.49	0.00	0.11	110.6	28.5	I.S.
Chloroform	4.80	0.259	0.69	0.44	0.00	61.2	26.7	I.S.
Tetrahydrofuran	7.58	0.207	0.55	0.00	0.55	66.0	26.4	I.S.
Dichloromethane	8.93	0.309	0.73	0.30	0.00	39.6	26.5	I.S.
Ethyl acetate	36.6	0.18	0.55	0.00	0.45	77.1	23.8	I.S.
Acetonitrile	45.60	0.460	0.75	0.19	0.40	82.0	19.1	I.S.
Isopropanol	49.20	0.570	0.48	0.76	0.84	82.6	23.0	I.S.
Butanol	50.20	0.600	0.47	0.84	0.84	117.4	24.2	I.S.
Ethanol	51.90	0.650	0.54	0.86	0.75	78.4	22.3	I.S.
Methanol	55.40	0.760	0.60	0.98	0.66	64.7	22.5	S
Formic acid	57.70	0.830	0.65	1.23	0.38	100.8	37.7	S
Hexafluoroisopropanol	65.30	1.070	0.65	1.96	0.00	58.2	16.1	S
Hexafluoroacetone-3H ₂ O	N.R.	N.R.	N.R.	N.R.	N.R.	-26.0 ^a	N.R.	S
Water	63.10	1.000	1.09	1.17	0.47	100.0	72.8	S

Table. 1.1. The properties of the non-aqueous solvents investigated for the dissolution of urea at a concentration of 100 mg/mL. Solvent parameters: dielectric constant (ϵ), Reichardt's parameter (E_T), and Kamlet-Taft parameters, π^* , α , and β . (N.R.) Not reported in the literature; ^a Hexafluoroacetone is a gas and it evaporates readily from aqueous solutions; (IS.) insufficiently soluble; and (S) sufficiently soluble.

The solubility of urea in the various solvents was clearly correlated to the parameters describing the bulk properties of the solvent (*i.e.*, the dielectric constant (ϵ) and Reichardt's parameter (E_T)). Indeed, solvents with dielectric constants and Reichardt's parameters similar to water were the most potent solvents for urea, and there was a threshold of dielectric constants and Reichardt's parameters below which the urea was insoluble (ca. 55 and 0.75, respectively). Interestingly, the Kamlet-Taft polarity parameters provided useful insight into the importance of individual molecular level interactions on the solubility of urea in the respective solvents. There was no clear correlation between the ability of a solvent to dissolve urea and the generalized polarity parameter, π^* . While solvents capable of dissolving urea all had π^* values of 0.60 or above, this was not a general rule: acetonitrile, chloroform, and dichloromethane (with π^* values of 0.75, 0.69 or 0.73 respectively) were poor/non-solvents. There was no correlation between the ability of a solvent to dissolve urea and its ability to accept hydrogen bonds (β). Hexafluoroisopropanol ($\beta = 0$) was an excellent solvent for urea whereas cyclohexane ($\beta = 0$) was a non-solvent for urea. The Kamlet-Taft parameter that gave the clearest insight into the ability of a solvent to dissolve urea was its ability to donate hydrogen bonds (α), and all of the solvents capable of dissolving urea had a values of ca. 1 or more. Although the solvent parameters for hexafluoroacetone hydrate are not reported in the literature, the acidity of the hydrate ($pK_a = 6.58$) make it a strong hydrogen bond donor capable of dissolving urea [25]. The solvents presented are clearly not an exhaustive list of those capable of dissolving urea at high concentrations, however our parameterized approach to investigating the ability of solvents to dissolve urea should enable others to easily identify other solvents for urea (or analogous sacrificial porogens).

Importantly, the solvents we found to be good solvents for urea (formic acid, hexafluoroisopropanol, hexafluoroacetone hydrate) are suitable for the dissolution of a variety of polymers (including clinically relevant polyesters, peptides, proteins,

polyurethanes, *etc.*) which significantly broadens the scope of biomaterials our methodology would be applicable for.

The Role of Solvent Choice on the Morphology of the Sacrificial Supracolloidal Porogens

Of the non-aqueous solvents identified as being capable of dissolving urea (*i.e.*, formic acid, hexafluoroacetone hydrate, hexafluoroisopropanol and methanol) we investigated formic acid, hexafluoroacetone hydrate and hexafluoroisopropanol in more detail (we omitted methanol because it is a non-solvent for silk and known to beta-sheet formation in the silk) [8-15].

Solvent evaporation from aqueous solutions of urea yields dendritic crystals if performed uncontrolled, or less dendritic and relatively well aligned crystals (over the length scale of a few hundred micrometers) if crystallization is initiated in a controlled fashion prior to evaporation using seeds of urea crystals [17]. Thus, we investigated urea crystallization from non-aqueous solvents under both uncontrolled and controlled evaporation conditions. Urea crystallization is controlled by the rate of evaporation of solvent from the solution of urea (100 mg/mL). Uncontrolled urea crystallization experiments were carried out by simply applying urea solutions to the surface of glass microscope slides and allowing the solvent to evaporate. Preliminary experiments attempting to control the directionality of urea crystallization were carried out by sealing the tip of a Pasteur pipette, adding a quantity of urea solution into the Pasteur pipette and allowing the solvent to evaporate slowly from the wide end.

Of the solvents investigated, formic acid was the solvent with the boiling point and surface tension closest to those of water, and we observed that uncontrolled urea crystallization yielded somewhat dendritic crystals, with sections that were relatively well aligned over the length scale of a few hundred micrometers (Figure 1.2A). Urea crystals formed from the uncontrolled evaporation of either hexafluoroacetone hydrate (Figure 1.2B) or hexafluoroisopropanol (Figure 1.2C) were less dendritic and showed alignment over the length scale of millimeters, although this was not free of defects. Interestingly, controlling the evaporation of hexafluoroisopropanol yielded crystals that were aligned over the length scale of centimeters (Figure 1.2D). Consequently, we conclude that the solvent-solute interactions govern not only the solubility of the solute, but also the morphology of the supracolloidal assemblies resulting from the evaporation of the solvent.

As the hierarchical supracolloidal assemblies act as sacrificial templates to generate porous biomaterials, we believe that it should be possible to tune the properties of such supracolloidal assemblies in a rational way that will enable the generation of biomaterials

instructing cells to assemble in complex biomimetic patterns (e.g., concentric lamellae observed in cortical bone, or helicoidal multi-lamellar alignment of corneal stroma tissue). Recent advances in supramolecular architectonics, particularly DNA-mediated interactions that have programmable structures from the Å to colloidal length scales suggest that we will see the first examples of these in the near future [26-32]. Moreover, the rational design of the constituent supramolecular building blocks [33-37] offers the prospect of precisely positioning functional species (e.g., nanoparticles) that may deliver therapeutics with precise spatial control, or sense and report changes in the properties of the surrounding tissues (e.g., clusters of nanoparticles whose optical properties change in response to chemical, electrical or mechanical triggers), which may be of use both *in vitro* and perhaps also *in vivo*.

Supracolloidal Temptation of Porous Silk Biomaterials

Urea is a well-known and widely utilized protein denaturant in aqueous solutions, and denatures proteins by disrupting the intermolecular and intramolecular hydrogen bonding interactions that cause proteins to fold or associate into hierarchical assemblies. While the uncontrolled crystallization of urea alone from formic acid yielded somewhat dendritic crystals with sections that were relatively well aligned over the length scale of a few hundred micrometers, the co-crystallization of urea and silk from formic acid, followed by washing to remove the urea, yielded silk-based films with dendritic crystal-templated pores with dimensions of ca. 200–400 μm (Figures 1.3A-B). Likewise, co-crystallization of urea and silk from hexafluoroacetone hydrate followed by washing also yielded silk-based films with very fine dendritic crystal-templated pores with dimensions of approximately 5-10 μm in diameter and up to 100 μm in length (Figure 1.33C-D). Co-crystallization of urea and silk from either hexafluoroisopropanol (Figure 1.3E) or water (Figure 1.3F) followed by washing yielded foams with larger pore diameters (10-40 μm) and lengths extending several hundred micrometers. These results suggest that molecular level interactions between the polymer and sacrificial template (in this case hydrogen bonding interactions between the silk and urea), and bulk solvent parameters (e.g., boiling point) play a role in dictating the morphology of the macroscopic pore structures within biomaterials generated in this fashion. Evidence for which can be observed in the predominantly dendritic pore structures in foams derived from formic acid and hexafluoroacetone hydrate instead of the more linear pore structures in foams derived from hexafluoroisopropanol or water. In the future we foresee prospects for tuning the polymer-pore interactions that will facilitate rational design of pore structure within biomaterials (particularly if DNA-architectonics were employed) [26-32].

Finally, to demonstrate that the pores imparted to silk-based biomaterials by supracolloidal assemblies of urea act as topographical guidance cues for cells cultured inside them, we cultured human dermal fibroblasts in water-derived scaffolds for five days. Obtaining images of the live cells inside the scaffolds using the common cell-permeant dye Calcein AM was challenging because of the strong background fluorescence of the scaffolds, however, it was possible to obtain markedly improved images of the cells inside the scaffolds after fixing them and staining with 4',6-diamidino-2-phenylindole (DAPI) (nuclei) and Alexa Fluor 488® Phalloidin (actin filaments), and we observed that the fibroblasts preferentially aligned with the pores inside the scaffold (Figure 1.4).

Experimental Section

Materials

Unless otherwise stated, all chemicals for synthesis and physicochemical analysis were of American Chemical Society (ACS) grade, purchased from Sigma-Aldrich (St Louis, MO, USA) and used as received without further purification. *Bombyx mori* silkworm fibroin was purchased from eBay. Reagents for cell culture were purchased from Invitrogen (Carlsbad, CA, USA) unless otherwise noted.

Urea Crystallization from Non-Aqueous Solvents

Urea was added to a non-aqueous solvent at a concentration of 0.1 g/mL. Samples were shaken in airtight containers (typically 15 or 50 mL centrifuge tubes) at 1000 rpm using a Thermomixer C (Eppendorf International, Hauppauge, NY, USA) for 48 h after which they were visually assessed to determine if the urea was soluble. Optically clear solutions were pipetted onto glass microscope slides (width 2.5 cm, length 7.5 cm) using disposable transfer pipettes. The solvent was allowed to evaporate in a fume hood at room temperature for 48 h and then dried under vacuum in a desiccator for 24 to 48 h. Preliminary experiments attempting to control the directionality of urea crystallization were carried out by sealing the tip of a Pasteur pipette, pipetting 200 μ L of solution into the vertical Pasteur pipette and allowing the solvent to evaporate slowly from the wide end. Images are representative of at least 3 locations on 3 samples.

Urea crystal Templating of Porous Silk-Based Films

Silk (2 g) and urea (2 g) were dissolved in either formic acid (20 mL) or hexafluoroacetone trihydrate (20 mL). Samples were shaken in airtight centrifuge tubes (50 mL) at 1000 rpm using a Thermomixer C until the components had fully dissolved (typically 24 to 48 h). Optically clear solutions of urea were pipetted onto glass microscope slides (width 2.5 cm, length 7.5 cm) using disposable transfer pipettes. The solvent was allowed to

evaporate in a fume hood at room temperature for 48 h and then dried under vacuum in a desiccator for 24 to 48 h.

Silk-based samples were immersed in aqueous methanol (80% methanol) for 1 h to assure that the silk was rendered water insoluble due to the formation of inter- and intra-molecular β -sheets, and then placed in a container of water to wash out urea and methanol. The samples were washed with water for 3 days to remove any traces of urea, typically exchanging the water every 3 h (*i.e.*, ca. 24 times), after which they were dried under high vacuum for 24 to 48 h.

Preparation of Silk-Based Tissue Scaffolds with Aligned Pores

Solutions of silk and urea in hexafluoroisopropanol were prepared as described in Section 2.2. Polydimethylsiloxane (PDMS) templates [18] were placed on flat rigid surfaces, and solutions of silk/urea were pipetted into the grooves using disposable transfer pipettes. Glass microscope slides (width 2.5 cm, length 7.5 cm) were placed on top of the PDMS templates and the solvent was allowed to evaporate (typically 144 h), after which the slides were removed and the silk/urea composites were then dried under vacuum in a desiccator for 24 to 48 h. Samples were immersed in aqueous methanol (80% methanol) for 1 h to assure that the silk was rendered water insoluble due to the formation of inter- and intra-molecular β -sheets, and then placed in a container of water to wash out urea and methanol. The samples were washed with water for 3 days to remove any traces of urea, typically exchanging the water every 3 h (*i.e.*, ca. 24 times), after which they were dried under high vacuum for 24 to 48 h. The resulting white silk-based tissue scaffolds had thicknesses of ca. 0.4 mm as determined using high precision digital calipers (ThermoFisher Scientific, Waltham, MA, USA), widths of ca. 2 mm, and pores aligned over lengths of up to 0.5 cm. Samples were cut to lengths appropriate for the various subsequent experiments using a razor blade.

Optical Microscopy of Urea and Silk Materials

Brightfield images of crystals of urea cast from formic acid, hexafluoroacetone hydrate and hexafluoroisopropanol, or porous silk-based materials were obtained using an Olympus 1X70 inverted microscope (Olympus Corporation of the Americas Inc., Center Valley, PA, USA) equipped with an Olympus DP80 dual color and monochrome digital camera (a 1.4 megapixel Bayer mosaic color CCD camera) that was attached to the microscope with a 0.63 B-mount. Image Analysis was performed using Olympus cellSens[®] imaging software, Version 1.11 (Olympus Corporation of the Americas Inc.). Images are representative of at least 3 locations on 3 samples.

Scanning Electron Microscopy (SEM)

Images of porous silk-based materials obtained using a scanning electron microscope (SEM). Samples were mounted on a SEM stub and sputter coated with Pt/Pd (15 nm) using a Cressington 208 benchtop sputter coater (Cressington Scientific Instruments, Watford, UK). All samples were imaged using a Zeiss Supra 40 VP field emission scanning electron microscope. Images are representative of at least 3 locations on 3 samples.

In Vitro Cell Culture

Human dermal fibroblasts (HDF, Invitrogen) were cultured in high glucose Dulbecco's Modified Eagle Medium (DMEM) supplemented with GlutaMAX™ Supplement (Invitrogen), 10% fetal bovine serum (FBS), and 1% penicillin/streptomycin antibiotic (Invitrogen). Cells were maintained at 37 °C in humidified atmosphere of 5% CO₂. HDF were seeded on the silk scaffold after treatment in ethanol for 1 h. Samples were subsequently rinsed three times in PBS and incubated in complete media before seeding. HDF were seeded at a density of 50,000 cells/cm² and cultured for 1 week. Calcein AM staining of live cells was applied in accordance with the instructions supplied with the kit (Invitrogen).

To stain the actin filaments and nuclei within cells, HDF were fixed in 2.5% paraformaldehyde in PBS at room temperature for 20 min, and then rinsed in PBS three times for 5 min. Cells were permeabilized in ice cold acetone (Sigma) at -20 °C for 5-10 min, and then rinsed in PBS three times. Samples were incubated in 4',6-diamidino-2-phenylindole (DAPI) solution at 300 nM for 10 min and for 1 h in 1:1000 Alexa Fluor® 488 Phalloidin (Invitrogen), followed by rinsing. Samples were imaged with a Keyence Fluorescence Microscope BZ-X700 (Keyence Corporation of America, Itasca, IL, USA) with excitation and emission filters at 495-518 nm for Alexa Fluor® 488 and 358-461 nm for DAPI. Images are representative of at least 3 locations on 3 samples.

Conclusions

Porous biomaterials are widely used in drug delivery and tissue engineering. 3D printing technologies are very promising for the preparation of porous biomaterials, however, they tend to be expensive. The removal of sacrificial templates (*e.g.*, colloidal crystals, ice crystals, fibers) from a matrix is a comparatively low cost alternative that allows the generation of hierarchically organized pores in biomaterials. Herein, we expand our studies on the use of sacrificial supracolloidal templates for the generation of porous biomaterials. We expand the scope of polymers that the methodology is compatible with by elucidating the solvent interactions governing the solubility of urea. We highlight the role of solvent

interactions on the morphology of the resulting supracolloidal crystals. We also highlight the role of polymer-urea interactions on the morphology of the pores in the resulting biomaterials. Finally, we demonstrate that it is possible to use our urea templating methodology to prepare *B. mori* silk protein-based biomaterials with pores that human dermal fibroblasts respond to by aligning with the long axis of the pores. We believe that our methodology has potential for application in a variety of different tissue engineering niches in which cell alignment is observed, including skin, bone, muscle and nerve; particularly when combined with the potential to guide the directionality of the urea crystals over multiple centimeters [18].

References for Example 1

1. Lutolf, M.P.; Hubbell, J.A. Synthetic biomaterials as instructive extracellular microenvironments for morphogenesis in tissue engineering. *Nat. Biotechnol.* 2005, 23, 47-55.
2. Edalat, F.; Sheu, I.; Manoucheri, S.; Khademhosseini, A. Material strategies for creating artificial cell-instructive niches. *Curr. Opin. Biotechnol.* 2012, 23, 820-825.
3. Rice, J.J.; Martino, M.M.; De Laporte, L.; Tortelli, F.; Briquez, P.S.; Hubbell, J.A. Engineering the regenerative microenvironment with biomaterials. *Adv. Healthc. Mater.* 2013, 2, 57-71.
4. Custodio, C.A.; Reis, R.L.; Mano, J.F. Engineering biomolecular microenvironments for cell instructive biomaterials. *Adv. Healthc. Mater.* 2014, 3, 797-810.
5. Rockwood, D.N.; Preda, R.C.; Yucel, T.; Wang, X.; Lovett, M.L.; Kaplan, D.L. Materials fabrication from *Bombyx mori* silk fibroin. *Nat. Protoc.* 2011, 6, 1612-1631.
6. Torres-Rendon, J.G.; Femmer, T.; De Laporte, L.; Tigges, T.; Rahimi, K.; Gremse, F.; Zafarnia, S.; Lederle, W.; Ifuku, S.; Wessling, M.; *et al.* Bioactive gyroid scaffolds formed by sacrificial templating of nanocellulose and nanochitin hydrogels as instructive platforms for biomimetic tissue engineering. *Adv. Mater.* 2015, 27, 2989-2995.
7. Sutherland, T.D.; Young, J.H.; Weisman, S.; Hayashi, C.Y.; Merritt, D.J. Insect silk: One name, many materials. *Annu. Rev. Entomol.* 2010, 55, 171-188.
8. Hardy, J.G.; R5mer, L.M.; Scheibel, T.R. Polymeric materials based on silk proteins. *Polymer* 2008, 49, 4309-4327.
9. Kundu, B.; Rajkhowa, R.; Kundu, S.C.; Wang, X. Silk fibroin biomaterials for tissue regenerations. *Adv. DrugDeliv. Rev.* 2013, 65, 457-470.

10. Hardy, J.G.; Scheibel, T.R. Composite materials based on silk proteins. *Prog. Polym. Sci.* 2010, *35*, 1093-1115.
11. Preda, R.C.; Leisk, G.; Omenetto, F.; Kaplan, D.L. Bioengineered silk proteins to control cell and tissue functions. *Methods Mol. Biol.* 2013, *996*, 19-41.
12. Hardy, J.G.; Scheibel, T.R. Production and processing of spider silk proteins. *J. Polym. Sci. A Polym. Chem.* 2009, *47*, 3957-3963.
13. Schacht, K.; Scheibel, T. Processing of recombinant spider silk proteins into tailor-made materials for biomaterials applications. *Curr. Opin. Biotechnol.* 2014, *29*, 62-69.
14. Widhe, M.; Johansson, J.; Hedhammar, M.; Rising, A. Invited review current progress and limitations of spider silk for biomedical applications. *Biopolymers* 2012, *97*, 468-478.
15. Hardy, J.G.; Scheibel, T.R. Silk-inspired polymers and proteins. *Biochem. Soc. Trans.* 2009, *37*, 677-681.
16. Moffat, J.R.; Seeley, G.J.; Carter, J.T.; Burgess, A.; Smith, D.K. Nanostructured polymers with embedded self-assembled reactive gel networks. *Chem. Commun.* 2008, 4601-4603.
17. Zawko, S.A.; Schmidt, C.E. Crystal templating dendritic pore networks and fibrillar microstructure into hydrogels. *Acta Biomater.* 2010, *6*, 2415-2421.
18. Hardy, J.G.; Cornelison, R.C.; Sukhvasi, R.C.; Saballos, R.J.; Vu, P.; Kaplan, D.L.; Schmidt, C.E. Electroactive tissue scaffolds with aligned pores as instructive platforms for biomimetic tissue engineering. *Bioengineering* 2015, *2*, 15-34.
19. Lan, Y.; Corradini, M.G.; Liu, X.; May, T.E.; Borondics, F.; Weiss, R.G.; Rogers, M.A. Comparing and correlating solubility parameters governing the self-assembly of molecular gels using 1,3:2,4-dibenzylidene sorbitol as the gelator. *Langmuir* 2014, *30*, 14128-14142.
20. Lan, L.; Corradini, M.G.; Rogers, M.A. Do molecular gelators cluster in hansen space? *Cryst. Growth Des.* 2014, *14*, 4811-4818.
21. Hirst, A.R.; Smith, D.K. Solvent effects on supramolecular gel-phase materials: Two-component dendritic gel. *Langmuir* 2004, *20*, 10851-10857.
22. Hardy, J.G.; Hirst, A.R.; Ashworth, I.; Brennan, C.; Smith, D.K. Exploring molecular recognition pathways within a family of gelators with different hydrogen bonding motifs. *Tetrahedron* 2007, *63*, 7397-7406.
23. Edwards, W.; Lagadec, C.A.; Smith, D.K. Solvent-gelator interactions-using empirical solvent parameters to better understand the self-assembly of gel-phase materials. *Soft*

- Matter* 2011, 7,
110-117.
24. Hardy, J.G.; Hirst, A.R.; Smith, D.K. Exploring molecular recognition pathways in one- and two-component gels formed by dendritic lysine-based gelators. *Soft Matter* 2012, 8, 3399-3406.
 25. Rajan, R.; Awasthi, S.K.; Bhattacharjya, S.; Balaram, P. "Teflon-coated peptides": Hexafluoroacetone trihydrate as a structure stabilizer for peptides. *Biopolymers* 1997, 42, 125-128.
 26. Aldaye, F.A.; Palmer, A.L.; Sleiman, H.F. Assembling materials with DNA as the guide. *Science* 2008, 321, 1795-1799.
 27. Carneiro, K.M.; Avakyan, N.; Sleiman, H.F. Long-range assembly of DNA into nanofibers and highly ordered networks. *Wiley Interdiscip. Rev. Nanomed. Nanobiotechnol.* 2013, 5, 266-285.
 28. McLaughlin, C.K.; Hamblin, G.D.; Sleiman, H.F. Supramolecular DNA assembly. *Chem. Soc. Rev.* 2011, 40, 5647-5656.
 29. Lin, N.; Liu, X.Y. Correlation between hierarchical structure of crystal networks and macroscopic performance of mesoscopic soft materials and engineering principles. *Chem. Soc. Rev.* 2015, doi:10.1039/C5CS00074B.
 30. Lo, P.K.; Mettera, K.L.; Sleiman, H.F. Self-assembly of three-dimensional DNA nanostructures and potential biological applications. *Curr. Opin. Chem. Biol.* 2010, 14, 597-607.
 31. Stulz, E. DNA architectonics: Towards the next generation of bio-inspired materials. *Chemistry* 2012, 18, 4456-4469.
 32. Jaeger, L.; Chworos, A. The architectonics of programmable RNA and DNA nanostructures. *Curr. Opin. Struct. Biol.* 2006, 16, 531-543.
 33. Jacobs, W.M.; Oxtoby, D.W.; Frenkel, D. Phase separation in solutions with specific and nonspecific interactions. *J. Chem. Phys.* 2014, 140, 204109.
 34. Jacobs, W.M.; Reinhardt, A.; Frenkel, D. Rational design of self-assembly pathways for complex multicomponent structures. *PNAS* 2015, 112, 6313-6318.
 35. Frenkel, D. Why colloidal systems can be described by statistical mechanics: some not very original comments on the Gibbs paradox. *Mol. Phys.* 2014, 112, 2325-2329.

36. Ciesielski, A.; Palma, C.A.; Bonini, M.; Samori, P. Towards supramolecular engineering of functional nanomaterials: Pre-programming multi-component 2D self-assembly at solid-liquid interfaces. *Adv. Mater.* 2010, 22, 3506-3520.
37. Guo, R.; Mao, J.; Xie, X.M.; Yan, L.T. Predictive supracolloidal helices from patchy particles. *Sci. Rep.* 2014, 4, 7021.

Example 2:

Bodily tissues are hierarchically structured composite materials with tissue-specific chemical and topographical properties, and these tissue-specific properties are known to act as cues (individually or in concert) that dictate the behavior of cells that inhabit them, and can potentially be engineered into instructional tissue scaffolds to achieve similar results [1-15]. Further to these cues, endogenous electric fields have been shown to act as behavioral cues during embryogenesis and wound healing, and devices that deliver exogenous electrical fields to the brain, ear or eye are already used in the clinic [4,16-19].

The complex interplay of chemical, electrical and topographical cues dictate the behavior of cells, and implantable biomaterials that act as instructional tissue scaffolds may facilitate the regeneration of functional tissues [2,7,8,12]. Topographical control of cell alignment is clearly observable within anisotropically aligned pores that are observed in bone [20,21], cardiac [22-25], nerve [3] and other tissues [6,7,26,27], which motivates the development of novel methodologies of imparting biomimetic porous structures within biomaterials.

While 3D printing technologies have prospects for the generation of porous materials, it is still challenging to fabricate porous structures that accurately mimic the chemical and intricate microscale and nanoscale topographical properties of native tissues, although solutions to these challenges are the subject of intense current research [28-31]. The removal of sacrificial templates embedded within a matrix (e.g., colloidal crystals, ice crystals, electrospun fibers) is another approach that allows the generation of hierarchically organized pore structures within materials [6,22].

Urea is a cheap, non-toxic solid that self-assembles through hydrogen bonding interactions (Figure 2.1). The evaporation of water from aqueous solutions of urea yields dendritic crystals if performed uncontrolled, and seeds of urea crystals can initiate crystallization in a controlled manner prior to solvent evaporation to obtain less dendritic and relatively well aligned crystals over the length scale of a few hundred micrometers [32].

Zawko and coworkers reported the use of a sacrificial supramolecular polymer-based crystal template (urea) to impart pores [32] within photocrosslinkable biopolymer-based hydrogels that typically have mechanical properties similar to soft tissues such as those in the central nervous system [33]. Uncontrolled urea crystallization in aqueous solutions of photocrosslinkable biopolymers followed by crosslinking yielded hydrogels with dendritic pores within them [32]. Carefully controlling the seeding of urea crystal formation followed by crosslinking allowed the generation of pores that were less dendritic and relatively aligned over the length scale of a few hundred micrometers. Interestingly, fibroblasts cultured within the gels were observed to align parallel to the fibrillar microstructure of the hydrogels, whereas keratinocytes did not display any preferential orientation in response to the topographical cue [32].

Manufacturing materials using entirely aqueous processes, such as that described above is an appealing prospect, but it limits the selection of the materials usable used to those that are soluble in water (e.g., polysaccharides), and there are many devices used in the clinic based on polymers that are insoluble in water (e.g., PCL). Here we report the use of urea-based supramolecular polymer crystals as sacrificial templates in the preparation of porous tissue scaffolds from non-aqueous solvents. Moreover, we report a simple scalable methodology for aligning the supramolecular polymer crystals that allows the generation of aligned pores within the matrix of biodegradable polymer; and demonstrate that the pores serve as topographical cues to which cells respond by aligning. Generation of an interpenetrating network of PPy within the scaffold renders the scaffolds electroactive and facilitates the electrical stimulation of cells cultured on the scaffolds. These methodologies are broadly applicable to a variety of materials, and represent broad platform technologies for biomimetic tissue engineering.

Porous biomaterials are broadly applicable in tissue engineering [6,7,26,27,34], and we sought to demonstrate that electroactive materials generated using our methodology can electrically stimulate cells to yield a response [8,35-46]. Therefore, we used our methodologies to manufacture electroactive PCL-based scaffolds with biomimetic topographical properties, and showed that electrical stimulation of glial cells from the peripheral nervous system (*i.e.*, Schwann cells) cultured on the scaffolds upregulated the production of nerve growth factor (NGF) which has been shown to promote peripheral nerve regeneration *in vivo* [47-64].

Experimental Section

Materials

Unless otherwise stated, all chemicals for synthesis and physicochemical analysis were of ACS grade, purchased from Sigma-Aldrich and used as received without further purification. Reagents for cell culture were purchased from Invitrogen (Carlsbad, CA, USA) unless otherwise noted. Neonatal rat Schwann cells isolated from sciatic nerves were purchased from ScienCell (Carlsbad, CA, USA).

Preparation of polydimethylsiloxane (PDMS) Templates

A 50 W laser cutter (Universal Laser Systems model VLS6.60, Scottsdale, AZ) was used to manufacture acrylic master templates with grooves 2 mm in depth, 2 mm in width and 10 cm long (Figures 2.2A and 2.2B). Polydimethylsiloxane (PDMS) was prepared using a Sylgard® 184 silicone elastomer kit in accordance with the manufacturer's protocol. The PDMS precursors were mixed in a disposable plastic weigh boat using a disposable plastic 1 mL pipette tip prior to being slowly poured over the grooved acrylic templates housed in a disposable container of aluminum foil. Thereafter this setup was stored under vacuum in a desiccator for 4 days at room temperature to allow the PDMS to crosslink fully. The acrylic templates were cut out of the resulting PDMS films using a razor blade and the PDMS was peeled from the acrylic template allowing it to be reused (Figure 2.2C).

Preparation of PCL-Based Tissue Scaffolds with Aligned Pores

PCL (Mn 80 kDa, 1 g) and urea (1 g) were dissolved in hexafluoroisopropanol (10 mL). Samples were shaken in airtight centrifuge tubes (50 mL) at 1000 rpm using a Thermomixer C (Eppendorf International, Hauppauge, NY) until the components had fully dissolved (typically 24 to 48 h). PDMS templates were placed on flat rigid surfaces, and optically clear hexafluoroisopropanol solutions of PCL/urea were pipetted into the grooves using disposable transfer pipettes. Glass microscope slides (width 2.5 cm, length 7.5 cm) were then placed on top of the PDMS templates (as depicted in Figure 2D) and the hexafluoroisopropanol was allowed to evaporate (typically 72 h), after which the slides were removed and the PCL/urea composites were placed in a container of water (100 mL). The samples were washed with water to remove the urea, exchanging the water every 3 h for 3 days, after which they were dried under high vacuum. The dimensions of the resulting white PCL-based tissue scaffolds had thicknesses of ca. 0.4 mm as were determined using high precision digital calipers (ThermoFisher Scientific, Waltham, MA), widths of ca. 2 mm, and pores aligned over lengths of up to 6.6 cm. Samples were cut to lengths, appropriate for the

various subsequent experiments, using a razor blade. The porosity of the samples can be calculated from:

$$\text{Porosity (\%)} = \left(\frac{\text{volume of urea}}{\text{volume of PCL} + \text{urea}} \right) * 100$$

The samples had mass ratios 1:1 PCL:urea. The density of PCL is: 1.145 g/cm³, and 1 g therefore occupies 0.8733 cm³. The density of urea is: 1.32 g/cm³; so 1 g occupies 0.7575 cm³. Assuming that all of the urea is leached during the washing process, the porosity is: 46.4 %.

Preparation of Electroactive PCL-Based Tissue Scaffolds with Aligned Pores

Pyrrrole was purified by passage over basic alumina. White PCL-based tissue scaffolds with aligned pores were placed in disposable 50 mL centrifuge tubes containing a solution of pyrrole (291 μL, [84 mM], 1 eq.) and PSS (Mn 70 kDa, 0.799 g, [84 mM], 1 eq.) in distilled water (50 mL). Samples were sonicated for 5 minutes and cooled to 4 °C (for 1 hour). Thereafter, ferric chloride (1.848 g, [228 mM], 2.7 eq.) was added. The samples were shaken to assure dissolution of the ferric chloride and then incubated for a further 24 h at 4 °C. Black electroactive tissue scaffolds with aligned pores were removed from the reaction mixture, placed in fresh distilled water, sonicated for 5 min, and then exhaustively washed (to remove monomers, oligomers and initiators) with deionized water until the water used to wash the materials was clear, colorless and the pH was neutral (ca. 48 h). Electroactive tissue scaffolds (PCL with an interpenetrating network of PPy and PSS) with aligned pores were dried under high vacuum at 21 °C. Samples were cut to lengths appropriate for the various subsequent experiments using a razor blade.

Scanning Electron Microscopy (SEM)

Images of porous PCL-based materials obtained using a scanning electron microscope (SEM). Samples were mounted on a SEM stub and sputter coated with Pt/Pd (15 nm) using a Cressington 208 benchtop sputter coater. All samples were imaged using a Zeiss Supra 40 VP field emission SEM.

Electrical Sheet Resistance

The electrical sheet resistance of the electroactive tissue scaffolds with aligned pores was measured in accordance with the method described by Schmidt [65] and Zhang [66]. In short, resistance (R in Ω) was measured between the two silver electrodes using a digital multimeter (DM-8A, Sperry Instrument, Milwaukee, WI). Sheet resistance (Rs) in Ω/square was calculated as follows:

$$R_s = R/W/L$$

where W is the sample width (in cm) and L is the distance between the two silver electrodes (in cm). The electrodes were moved to different positions after each measurement, and the resistance R was recorded in at least ten different positions on the materials.

Fourier Transform Infrared Spectroscopy (FTIR)

Infrared spectroscopy was carried out on the samples to confirm that the surface chemistry of the scaffolds had changed after the growth of an interpenetrating network of PPy and PSS within the PCL matrix. A Thermo Scientific Nicolet 380 FTIR Spectrometer (Thermo Fisher Scientific Inc., USA) was used. Spectra were recorded in attenuated total reflectance (ATR) mode at 21 °C with a 1 cm^{-1} resolution and 128 scans (corrected for background and atmosphere using OMNIC software provided with the spectrometer). Samples were secured in position on the ATR crystal using the built-in clamp.

X-Ray Photoelectron Spectroscopy (XPS)

XPS was carried out on the samples to confirm that the surface chemistry of the scaffolds had changed after the growth of an interpenetrating network of PPy and PSS within the PCL matrix. XPS was performed on a Kratos Axis X-ray photoelectron spectrometer (Kratos Analytical Ltd., Manchester, UK). The binding energy was calibrated using the C 1s photoelectron peak at 284.6 eV as a reference. The CasaXPS computer program was used for peak fitting of the C 1s and O 1s peaks in the XPS spectra. The reported spectra are representative of two measurements at different positions on a sample.

In Vitro Degradation Study

Samples were incubated in PBS (1 mL) at 37 °C, in the absence or presence of cholesterol esterase (4 units/mL, Sigma Aldrich, USA). At specific time points the buffer was removed, the samples were carefully washed with deionized water. The samples were then dried under high vacuum to obtain a dry weight. The buffer (with or without enzymes) was replaced, and the mass of the film was recorded over a period of several days. Mass loss profiles represent the average of at least five samples.

In Vitro Cell Culture

PCL-Based Tissue Scaffold Preparation and Sterilization

Commercially available tissue-culture treated Corning® Costar® tissue culture plates were used for control experiments. Non-electroactive and electroactive PCL-based tissue scaffolds with aligned pores were incubated in an aqueous solution of poly-D-lysine (PDL, 50 µg/mL) for 1 hour and then washed thoroughly with sterile water to remove any weakly adsorbed PDL (exchanging the water every 10 min for 1 h). Samples were inserted in

untreated polystyrene tissue culture plates and sterilized by incubation in 70% ethanol followed by exposure to UV for 60 min.

In Vitro Culture of Schwann Cells

After sterilization, scaffolds were incubated for 30 min under 3 mm of medium. Schwann cell growth medium was composed of: 25.5 mL of low glucose Dulbecco's Modified Eagle Medium (DMEM); 8.5 mL of GIBCO® Ham's F-12 Nutrient Mixture; 350 μ L Penicillin Streptomycin (1% of the final volume); 350 μ L N2 supplement (2% of the final volume); Forskolin [5 μ M]; Neuregulin-1 β (50 ng/nL). Medium was aspirated and replaced prior to Schwann cell seeding at 5,000 cells/cm² under 3 mm of medium, and incubated at 37 °C, 95% humidity, and 5% CO₂. Cell viability before starting the experiment was determined by the Trypan Blue (Sigma, USA) exclusion method, and the measured viability exceeded 95% in all cases. After 2 days the medium was aspirated, the scaffolds were washed gently with PBS, and the cells were fixed with 4% paraformaldehyde in PBS for 15 min. The scaffolds were washed again with PBS (3 \times 1 mL) and stored at 4 °C until they were stained and imaged.

Electrical Stimulation of Schwann Cells

Electrical stimulation of Schwann cells was achieved employing a custom built setup. Non-conductive glass slides, polycarbonate wells (square polycarbonate blocks, thickness of 1 cm, sides of 2.5 cm, with square holes with sides of 0.9 cm cut out), [67,68] Dow Corning® high vacuum grease, and medium binder clips (Staples®, Framingham, MA) were sterilized by autoclaving. Holes were drilled into the sides of 10 cm polystyrene Petri dishes using a Dremel saw (Lowe's, Mooresfield, NC, USA), and the plates were sterilized by exposure to UV for 60 min. Adhesive-backed copper tape (5 mm width, Ted Pella, Inc.), waterproof Kapton® tape (1 cm width, Fisher Scientific, Waltham, MA, USA), wires and alligator clips were sterilized by exposure to UV for 60 min.

Electroactive PCL-based tissue scaffolds with aligned pores (prepared as described in 2.1.1.1.) were placed on glass slides and secured in position with two thin strips of adhesive-backed copper tape that were attached to the films, parallel to one another and separated by a distance of ca. 4 cm. One face of the polycarbonate wells was coated with vacuum grease and placed on the electroactive tissue scaffolds, greased side down, in contact with the glass slide. A binder clip on either side of the well was used to secure this in position and render it water tight. A strip of copper tape was run between the parallel copper strips attached to the scaffolds and the ends of the slides as points of contact for the alligator clip-terminated wires attached to the multipotentiostat (CH Instruments, Austin, TX, USA). The counter and

reference electrodes were connected together and clipped to copper tape on one side of the slide, and the working electrode was clipped to copper tape on the other side of the slide. Schwann cells were plated and cultured as described in section 2.13.3. A potential step of +50 mV/mm was placed across the substrate for the duration of 1 h [69-71], after which the wires were disconnected and the substrates cultured as normal (see Figure 2.3).

Fluorescence Staining and Imaging of Cells

Cells fixed with paraformaldehyde were permeabilized with 0.1% Triton X-100 (Fluka) and 2% bovine serum albumin (BSA) in PBS buffer for 5 min, followed by blocking with 2% BSA in PBS buffer for 30 min at room temperature. Actin filaments and cell nuclei within cells were stained with Alexa Fluor 488[®] Phalloidin (Life Technologies, USA) for 30 min and 4',6-diamidino-2-phenylindole (DAPI, Invitrogen, USA) for 5 min, respectively. The cells were thereafter washed three times with PBS and stored at 4 °C until images were acquired. Fluorescence images of cells were obtained using an Olympus 1X70 inverted microscope equipped with an Olympus DP80 dual color and monochrome digital camera (a 1.4 megapixel Bayer mosaic color CCD camera) that was attached to the microscope with a 0.63 B-mount. Image Analysis was done using Olympus cellSens[®] imaging software, Version 1.1.1.

NGF secretion studies

Schwann cells were cultured under the conditions described above for 1 day, after which electrical stimulation for 1 h was optionally applied; non-stimulated controls included commercially available tissue-culture treated Corning[®] Costar[®] tissue culture plates, and non-electroactive/electroactive PCL-based tissue scaffolds with aligned pores. Medium was collected from the Schwann cell cultures immediately after electrical stimulation (0 h) and thereafter in intervals of 12 h for 3 days. The medium was stored at -20 °C for no more than 1 week prior to use in the Rat NGF ELISA Kit (Insight Genomics, Falls Church, VA, USA). ELISA kits were utilized in accordance with the protocol supplied with the kit, employing a Synergy HT Multi-Mode Microplate Reader (Biotek US, Winooski, VT, USA). Concentrations of NGF/mL were calculated based on standards supplied in the NGF ELISA Kit. Differences in cell numbers over the 3 day period of the assay were negligible as determined with an AlamarBlue[®] cell viability assay, and concentrations of NGF in pg/mL are therefore presented uncorrected.

Results and Discussion

Controlled Crystallization of Urea-Based Supramolecular Polymers as Sacrificial Templates for the Generation of Porous Biomaterials: Preparation and Characterization of PCL-Based Tissue Scaffolds with Highly Aligned Pores

We chose to produce tissue scaffolds incorporating aligned pores. With this goal in mind, we produced hard acrylic master templates with grooves with depths of 2 mm, widths of 2 mm and lengths of 10 cm using a laser cutter (Figure 2.2A). Flexible PDMS analogues were prepared by embedding the master template (Figure 2.2B) in a container with the PDMS precursors, allowing them to crosslink and then peeling the flexible PDMS template (Figure 2C) away from the surface of the acrylic master template. The resulting flexible PDMS templates with possessing grooves with widths and heights of 2 mm and lengths of 10 cm for the solutions of urea/polymer/hexafluoroisopropanol (Figure 2.2C, left) had an open top upon which a glass slide (width of 2.5 cm, length of 7.5 cm) was placed. The glass slide prevented hexafluoroisopropanol evaporation from the top of the template and allowed hexafluoroisopropanol evaporation only at either end of the glass slide-covered grooves (Figure 2.2D). Such The PDMS templates facilitated controlled solvent evaporation, preferential alignment of urea crystals within the grooves, and the resulting scaffolds to be easily removed from the templates to allow the sacrificial urea template to be removed by washing, yielding scaffolds with porosities of ca. 46.4 % .

PCL-based tissue scaffolds produced using this methodology had thicknesses of ca. 0.4 mm, widths of ca. 2 mm, and pores (with widths of 10s of micrometers as observed by SEM, Figure 2.4A and 2.4B) aligned over lengths of up to 6.6 cm (ca. 88% of the length of the glass slide used to cover the grooves), which are clinically relevant length scales [8,72]. It is noteworthy that this would be straightforward to adapt to manufacture longer scaffolds using longer flexible templates and covers, and that this a very simple and inexpensive methodology well suited to laboratories across the world.

Preparation and Characterization of Electroactive PCL-Based Tissue Scaffolds with Aligned Pores

Methodology for the Preparation of Electroactive PCL-Based Tissue Scaffolds

A simple method to reproducibly prepare electroactive PCL-based scaffolds was the generation of an interpenetrating network of electroactive PPy within the non-electroactive PCL matrix. The interpenetrating networks of PPy in PCL scaffolds were generated simply by incubating the scaffolds in aqueous solutions of pyrrole(monomer, concentration \leq 84 mM, PSS(dopant counter ion, 1 molar equivalent) and ferric chloride (initiator, 2.7 molar

equivalents) for 24 h followed by exhaustive washing. [65, 73] This simple process reproducibly produced mechanically stable electroactive tissue scaffolds with well-preserved micrometer and nanometer scale features; indeed, we found that use of higher concentrations of pyrrole (which is a good solvent for PCL) partially dissolved the PCL-based scaffolds, and extra crosslinking and washing steps are necessary to circumvent this problem (which also permits them to be sterilized by autoclaving) as reported by Yaszemski and co-workers [74-77]. Non-electroactive PCL-based scaffolds were white, whereas the electroactive scaffolds were black, and electron microscopy showed evidence of a slightly increased surface roughness on the nanometer scale due to the presence of polyelectrolyte complexes of positively charged PPy and negatively charged PSS interwoven with the PCL matrix (Figure 3C and 3D) [65].

Spectroscopic Analysis of Non-Electroactive and Electroactive PCL-Based Tissue Scaffolds

Comparison of infrared spectra recorded in ATR mode of the non-electroactive scaffolds (Figure 2.5A) and the electroactive scaffolds (Figure 2.5B) confirmed the successful generation of an interpenetrating network of polyelectrolyte complexes of positively charged PPy and negatively charged PSS interwoven within the PCL matrix. Indeed, the peaks observed in the spectra of the electroactive scaffolds at ca. 1543 and ca. 1480 cm^{-1} are characteristic of the antisymmetric and symmetric ring stretching modes respectively (Figure 2.5B) [78,79]. In addition, comparison of X-ray photoelectron spectra of the non-electroactive scaffolds (Figure 2.5C) and the electroactive scaffolds (Figure 2.5D) provided further evidence of alterations to the surface chemistry of the materials. The low intensity peak in the spectra at ca. 31 eV is the Na 2s and 2p peak (from NaCl), and the peak at ca. 500 eV is the corresponding Auger transition of sodium. The peak at ca. 99 eV is the Si 2p peak (a combination of the Si 2p 1 and Si 2p 3 peaks) from the underlying substrate. The peaks at ca. 285 eV correspond to C 1s, and the broad peak at ca. 531 corresponds to O 1s (a combination of C-O at ca. 531 and C=O at ca. 533) which all arise from the PCL backbone. The appearance of peaks in the spectra of the electroactive scaffolds at ca. 400 eV (N 1s) and ca. 168 eV (S 2p) are characteristic of PPy and PSS, respectively (Figure 2.5D) [65,66], confirming the successful generation of an interpenetrating network.

Electrical Properties of Electroactive PCL-Based Tissue Scaffolds

Generation of an interpenetrating network of polyelectrolyte complexes of PPy and PSS within the non electroactive PCL-based scaffolds rendered them electroactive with sheet resistances of ca. 68 k Ω /square, on the order of analogous PPy-PSS polyelectrolyte complex-

coated poly(lactic-co-glycolic acid) nanofibers (ca. 17 kH/square) [65] or PPy-heparin polyelectrolyte complex-coated Dacron[®] 56 polyester fibers (ca. 16 kH/square) [66]. The relatively low resistance of the PPy-modified poly(lactic-co-glycolic acid) or Dacron[®] 56 fibers is likely to be because the PPy is localized on the surface of the fibers [65], whereas the interpenetrating networks of PPy-PSS and PCL would have PPy-PSS in the bulk of the PCL and display some non-conductive PCL chains on the surface of the scaffolds [73].

In Vitro Degradation of Non-Electroactive and Electroactive PCL-Based Tissue Scaffolds

While *in vitro* degradation experiments do not accurately reproduce conditions that materials encounter when implanted *in vivo* (particularly patient-specific immune responses or the tissue-specific distribution of enzymes), they are useful to confirm the potential of materials to degrade upon exposure to enzymes found *in vivo*. To demonstrate that enzymatic/hydrolytic degradation of the non-electroactive and electroactive PCL-based tissue scaffolds is possible, we incubated them in PBS in the absence or presence of a high concentration of an enzyme known to hydrolyze ester bonds in polyesters, cholesterol esterase (4 units/mL) [80-84]. When incubated in PBS for 12 days the masses of non-electroactive and electroactive scaffolds did not change significantly (Figure 2.6A, 2.6B, respectively) because hydrolysis of PCL occurs very slowly [85]. The presence of the esterase increases the rate of hydrolysis, resulting in a notable mass loss, ca. 40% over 12 days, from the non-electroactive PCL-based scaffolds (Figure 2.6A) and ca. 50% from the electroactive versions (Figure 2.6B). The presence of the electroactive polyelectrolyte complex of PPy and PSS appears to increase the hydrophilicity of the scaffolds allowing the enzyme to more easily access the PCL chains. The scaffolds are likely to degrade slowly if administered *in vivo* (over the period of several years) in line with other PCL-based materials [86] leaving behind the residual water insoluble polyelectrolyte complex of PPy and PSS that preclinical trials have shown to be relatively non-immunogenic. Indeed, histological analyses of tissue in the vicinity of polypyrrole-based tissue scaffolds implanted subcutaneously or intramuscularly in rats showed immune cell infiltration comparable to FDA-approved poly(lactic acid-co-glycolic acid) [87] or poly(D,L-lactide-co-glycolide) [87]. Similarly, there was no significant inflammation in the vicinity of polypyrrole-based materials implanted in the coronary artery of rats after 5 weeks [88], sciatic nerve guidance channels implanted in rats after 8 weeks [89], or electrodes in rat brains after 3 or 6 weeks [90].

In Vitro Cell Culture Studies on Instructional PCL-Based Tissue Scaffolds

Topographical Instruction: Aligned Pores are a Topographical Cue that Cells Respond to by Aligning

The anisotropic features are commonly observed in functional tissues (including bone, cardiac, musculoskeletal and nervous tissues), and scaffolds with biomimetic architectures perform well in the clinic [2,7,8,12]. We investigated the adhesion of rat primary Schwann cells on the non-electroactive and electroactive PCL-based tissue scaffolds with highly aligned pores. After 48 h in culture we observed that Schwann cells responded to the topographical cue by aligning preferentially with the long axis of the pores in the scaffolds (Figures 2.7A-B), which is promising for future studies either with scaffolds derived from other polymers and using other cell types.

Electrical Instruction: Electrical Stimulation is a Cue that Schwann Cells Respond to by Increasing the Excretion of Nerve Growth Factor (NGF)

The role of endogenous electrical fields in the development of the nervous system motivated research into the application of exogenous electrical fields for therapeutic purposes, and preclinical studies show that electrical stimulation of damaged peripheral nerves for short periods of time (e.g., 1 h) improves their regeneration [18,69-71]. Electrical stimulation is known to affect cells differently depending upon a variety of factors including the cell type and species from which they were isolated, as discussed in detail in recent reviews [18,19]. Electrical stimulation of Schwann cells has been shown to increase the production of nerve growth factor (NGF) from Schwann cells cultured on electroactive indium tin oxide-based substrates [91], PPy-based substrates [92] or poly(3,4-ethylenedioxythiophene)-based substrates [93] or non-electroactive poly-L-Lysine-coated glass substrates [94]. NGF is a protein that plays a role in the growth, maintenance and survival of neurons. In fact, preclinical studies in rats showed that NGF promoted peripheral nerve regeneration [47-64], encouraging the development of NGF drug delivery systems [95], some of which are electrochemically triggered [96] and have the potential for regeneration of the nervous system.

Electroactive scaffolds such as those we report here clearly have the potential to act both as electrochemically-triggered drug delivery devices as well as instructive scaffolds that enable electrical stimulation of cells. We focused on the latter, investigating the amount of NGF expressed by rat Schwann cells when electrically stimulated (50 mV/mm) on the electroactive PCL-based tissue scaffolds with aligned pores, and non-stimulated controls including commercially available tissue-culture treated Corning® Costar® tissue culture plates, and non-electroactive/electroactive PCL-based tissue scaffolds with aligned pores. The concentration of NGF in the medium (in pg/mL) was determined using a Rat NGF ELISA Kit (Insight Genomics, Falls Church, VA) immediately after electrical stimulation and thereafter

in intervals of 12 h for 3 days. There were no significant differences in NGF production by Schwann cells in any of the non-stimulated controls over the 3 day study. In contrast to this, after 48 hours in culture we observed that Schwann cells responded to the electrical cue and increased production of NGF to ca. three times the amount produced by an equivalent number of cells without electrical stimulation, a trend that was markedly more apparent during the following 24 h (Figure 2.8). Such increases in NGF production have been shown to encourage neurite outgrowth from neurons in a number of studies [97,98].

Our finding that cells respond not only to the topographical cue imparted through use of urea-based supramolecular polymer crystal sacrificial templates, but also to the electrical cue facilitated by an interpenetrating network of PPy shows the potential of our innovative biomaterials to function not only as scaffolds with potential for nerve regeneration, but also as platforms for the development of porous scaffolds for other tissues.

Conclusions

There is a need for biomaterials with biomimetic chemical and topographical properties for application as tissue scaffolds. Likewise, materials that facilitate the application of exogenous electrical fields have a variety of potential therapeutic applications. Here we present a novel process to manufacture instructional tissue scaffolds with biomimetic topographical properties and a process to render these scaffolds electroactive that allows electrical stimulation of cells cultured on them.

Sacrificial supramolecular polymer-based crystals composed of urea were used to generate pores within a matrix of a biodegradable polymer. We show that it is possible to generate both dendritic and linear urea crystals dependent on the solvent used, and, moreover, that co-crystallization of urea with a polymer controls the propensity of the urea to form dendritic or linear crystals, thereby controlling the topography generated within the polymer matrix. Additionally, we have developed a simple, inexpensive, scalable method of aligning the supramolecular polymer-based crystals within the biodegradable polymer matrix, allowing the preparation of scaffolds with macroscopic pores that are aligned over long, clinically relevant distances on the order of centimeters. The pores act as topographical cues to which rat Schwann cells responded by aligning.

We can prepare electroactive tissue scaffolds with biomimetic topographical properties using simple chemistry that allows the electrical stimulation of Schwann cells cultured on the scaffolds. This electrical cue increased the production of nerve growth factor

(NGF) to more than three times the amount produced by non-stimulated cells, which may improve clinical outcomes during peripheral nerve regeneration.

Together, these simple, inexpensive methods represent a platform technology that facilitates the development of porous electroactive biomaterials.

References

1. Jaklenec A, Stamp A, Deweerd E, Sherwin A, Langer R. Progress in the tissue engineering and stem cell industry "are we there yet?". *Tissue Eng. Part B.* 2012;18(3):155-166. doi: 10.1089/ten.teb.2011.0553.
2. Harrison RH, St-Pierre J, Stevens MM. Tissue engineering and regenerative medicine: A year in review. *Tissue Eng. Part B.* 2014;20(1):1-16.
3. Wrobel MR, Sundararaghavan HG. Directed migration in neural tissue engineering. *Tissue Eng. Part B.* 2014;20(2):93-105. doi: 10.1089/ten.teb.2013.0233.
4. Balint R, Cassidy NJ, Cartmell SH. Electrical stimulation: A novel tool for tissue engineering. *Tissue Eng. Part B.* 2013; 19(1):48-57. doi: 10.1089/ten.teb.2012.0183.
5. Zhang BGX, Quigley AF, Myers DE, Wallace GG, Kapsa RMI, Choong PFM. Recent advances in nerve tissue engineering. *Int. J. Artif. Organs.* 2014;37(4):277-291. doi: 10.5301/ijao.5000317.
6. Ma PX. Biomimetic materials for tissue engineering. *Adv. Drug Deliver. Rev.* 2008;60(2):184-198. doi: 10.1016/j.addr.2007.08.041.
7. Lutolf MP, Hubbell JA. Synthetic biomaterials as instructive extracellular microenvironments for morphogenesis in tissue engineering. *Nat. Biotechnol.* 2005;23(1):47-55. doi: 10.1038/nbt1055.
8. Spivey EC, Khaing ZZ, Shear JB, Schmidt CE. The fundamental role of subcellular topography in peripheral nerve repair therapies. *Biomaterials.* 2012;33(17):4264-4276. doi: 10.1016/j.biomaterials.2012.02.043.
9. Dvir T, Timko BP, Kohane DS, Langer R. Nanotechnological strategies for engineering complex tissues. *Nat. Nanotechnol.* 2011;6(1): 13-22. doi: 10.1038/NNANO.2010.246.
10. Wang X, Yan Y, Zhang R. Recent trends and challenges in complex organ manufacturing. *Tissue Eng. Part B.* 2010;16(2): 189-197. doi: 10.1089/ten.teb.2009.0576.
11. Griffith LG, Swartz MA. Capturing complex 3D tissue physiology *in vitro*. *Nat. Rev. Mol. Cell Biol.* 2006;7(3):211-224. doi: 10.1038/nrml858.

12. Place ES, Evans ND, Stevens MM. Complexity in biomaterials for tissue engineering. *Nat. Mater.* 2009;8(6):457-470. doi: 10.1038/NMAT2441.
13. Fisher MB, Mauck RL. Tissue engineering and regenerative medicine: Recent innovations and the transition to translation. *Tissue Eng. Part B.* 2013;19(1): 1-13. doi: 10.1089/ten.teb.2012.0723.
14. Salgado AJ, Oliveira JM, Martins A, et al. Tissue engineering and regenerative medicine: Past, present, and future. *Tissue Engineering of the Peripheral Nerve: Stem Cells and Regeneration Promoting Factors.* 2013;108:1-33. doi: 10.1016/B978-0-12-410499-0.00001-0.
15. Berthiaume F, Maguire TJ, Yarmush ML. Tissue engineering and regenerative medicine: History, progress, and challenges. *Annu. Rev. Chem. Biomol. Eng., Vol 2.* 2011;2:403-430. doi: 10.1146/annurev-chembioeng-061010-114257.
16. Hardy JG, Lee JY, Schmidt CE. Biomimetic conducting polymer-based tissue scaffolds. *Curr. Opin. Biotechnol.* 2013;24(5):847-854. doi: 10.1016/j.dopbio.2013.03.011.
17. Rutten WLC. Selective electrical interfaces with the nervous system. *Annu. Rev. Biomed. Eng.* 2002;4:407-452. doi: 10.1146/annurev.bioeng.4.020702.153427.
18. Thompson DM, Koppes AN, Hardy JG, Schmidt CE. Electrical stimuli in the central nervous system microenvironment. *Annu. Rev. Biomed. Eng.* 2014;16:397-430.
19. Yue Z, Moulton SE, Cook M, O'Leary S, Wallace GG. Controlled delivery for neuro-bionic devices. *Adv. Drug Deliver. Rev.* 2013;65(4):559-569. doi: 10.1016/j.addr.2012.06.002.
20. Despang F, Bernhardt A, Lode A, et al. Synthesis and physicochemical, *in vitro* and *in vivo* evaluation of an anisotropic, nanocrystalline hydroxyapatite bisque scaffold with parallel-aligned pores mimicking the microstructure of cortical bone. *J. Tissue Eng. Regen. Med.* 2013;Apr 15.
21. Spoerke ED, Murray NGD, Li H, Brinson LC, Dunand DC, Stupp SI. Titanium with aligned, elongated pores for orthopedic tissue engineering applications. *J. Biomed. Mater. Res. Part A.* 2008;84A(2):402-412. doi: 10.1002/jbm.a.31317.
22. Davidenko N, Gibb T, Schuster C, et al. Biomimetic collagen scaffolds with anisotropic pore architecture. *Acta Biomater.* 2012;8(2):667-676. doi: 10.1016/j.actbio.2011.09.033.
23. Vejseli V, Lee EJ. Cardiac fibroblast-formed anisotropic decellularized engineered cardiac tissues. *2013 39th Annual Northeast Bioengineering Conference (NEBEC 2013).* 2013:127-128. doi: 10.1109/NEBEC.2013.4.

24. Kim D, Lipke EA, Kim P, et al. Nanoscale cues regulate the structure and function of macroscopic cardiac tissue constructs. *PNAS*. 2010;107(2):565-570. doi: 10.1073/pnas.0906504107.
25. Dunn DA, Hodge AJ, Lipke EA. Biomimetic materials design for cardiac tissue regeneration. *WIREs Nanomed. Nanobiotechnol.* 2014;6(1): 15-39. doi: 10.1002/wnan.1241.
26. Phillips JB. Building stable anisotropic tissues using cellular collagen gels. *Organogenesis*. 2014;10(1):6-8. doi: 10.4161/org.27487.
27. Nectow AR, Kilmer ME, Kaplan DL. Quantifying cellular alignment on anisotropic biomaterial platforms. *J. Biomed. Mater. Res. Part A*. 2014;102(2):420-428. doi: 10.1002/jbm.a.34713.
28. Zhu W, O'Brien C, O'Brien JR, Zhang LG. 3D nano/microfabrication techniques and nanobiomaterials for neural tissue regeneration. *Nanomedicine*. 2014;9(6):859-875. doi: 10.2217/NNM. 14.36.
29. Sayyar S, Cornock R, Murray E, Beirne S, Officer DL, Wallace GG. Extrusion printed graphene/polycaprolactone/composites for tissue engineering. *Materials Science Forum*. 2014;773-774:496-502. doi: 10.4028/www.scientific.net/MSF.773-774.496.
30. Ferris CJ, Gilmore KG, Wallace GG, Panhuis MIH. Biofabrication: An overview of the approaches used for printing of living cells. *Appl. Microbiol. Biotechnol.* 2013;97(10):4243-4258. doi: 10.1007/s00253-013-4853-6.
31. Ferris CJ, Gilmore KJ, Beirne S, McCallum D, Wallace GG, Panhuis MIH. Bio-ink for on-demand printing of living cells. *Biomater. Sci*. 2013;1(2):224-230. doi: 10.1039/c2bm00114d.
32. Zawko SA, Schmidt CE. Crystal templating dendritic pore networks and fibrillar microstructure into hydrogels. *Acta Biomater.*. 2010;6(7):2415-2421. doi: 10.1016/j.actbio.2010.02.021.
33. Seidlits SK, Khaing ZZ, Petersen RR, et al. The effects of hyaluronic acid hydrogels with tunable mechanical properties on neural progenitor cell differentiation. *Biomaterials*. 2010;31(14):3930-3940. doi: 10.1016/j.biomaterials.2010.01.125.
34. Zohora FT, Azim AMA. Biomaterials as porous scaffolds for tissue engineering applications: A review. *Eur. Sci. J.*. 2014;10(21):Zohora.
35. Subramanian A, Krishnan UM, Sethuraman S. Development of biomaterial scaffold for nerve tissue engineering: Biomaterial mediated neural regeneration. *J. Biomed. Sci*. 2009;16:108. doi: 10.1186/1423-0127-16-108.

36. Tresco PA. Tissue engineering strategies for nervous system repair. *Neural Plasticity and Regeneration*. 2000;128:349-363.
37. Saracino GAA, Cigognini D, Silva D, Caprini A, Gelain F. Nanomaterials design and tests for neural tissue engineering. *Chem. Soc. Rev.* 2013;42(1):225-262. doi: 10.1039/c2cs35065c.
38. Gu X, Ding F, Williams DF. Neural tissue engineering options for peripheral nerve regeneration. *Biomaterials*. 2014;35(24):6143-6156. doi: 10.1016/j.biomaterials.2014.04.064.
39. Geuna S, Gnani S, Perroteau I, Tos P, Battiston B. Tissue engineering and peripheral nerve reconstruction: An overview. *Tissue Engineering of the Peripheral Nerve: Stem Cells and Regeneration Promoting Factors*. 2013;108:35-57. doi: 10.1016/B978-0-12-410499-0.00002-2.
40. Marquardt LM, Sakiyama-Elbert SE. Engineering peripheral nerve repair. *Curr. Opin. Biotechnol.* 2013;24(5):887-892. doi: 10.1016/j.copbio.2013.05.006.
41. Angius D, Wang H, Spinner RJ, Gutierrez-Cotto Y, Yaszemski MJ, Windebank AJ. A systematic review of animal models used to study nerve regeneration in tissue-engineered scaffolds. *Biomaterials*. 2012;33(32):8034-8039. doi: 10.1016/j.biomaterials.2012.07.056.
42. Daly WT, Knight AM, Wang H, et al. Comparison and characterization of multiple biomaterial conduits for peripheral nerve repair. *Biomaterials*. 2013;34(34):8630-8639. doi: 10.1016/j.biomaterials.2013.07.086.
43. Hudson TW, Liu SY, Schmidt CE. Engineering an improved acellular nerve graft via optimized chemical processing. *Tissue Eng.* 2004;10(9-10): 1346-1358. doi: 10.1089/1076327042500319.
44. Hudson TW, Zawko S, Deister C, et al. Optimized acellular nerve graft is immunologically tolerated and supports regeneration. *Tissue Eng.* 2004; 10(11-12):1641-1651. doi: 10.1089/ten.2004.10.1641.
45. Hudson TW, Evans GRD, Schmidt CE. Engineering strategies for peripheral nerve repair. *Orthop. Clin. North Am.* 2000;31(3):485-498. doi: 10.1016/S0030-5898(05)70166-8.
46. Hudson TW, Evans GRD, Schmidt CE. Engineering strategies for peripheral nerve repair. *Clin. Plast. Surg.* 1999;26(4):617-628.

47. Ikegami R. Changes of nerve growth factor (NGF) content in injured peripheral nerve during regeneration: Local synthesis of NGF by Schwann cells. *Nihon Seikeigeka Gakkai zasshi*. 1990;64(7):612-22.
48. Yu H, Peng J, Sun H, et al. [Effect of controlled release nerve growth factor on repairing peripheral nerve defect by acellular nerve graft]. *Zhongguo Xiu Fu Chong Jian WaiKe Za Zhi*. 2008;22(1 1): 1373-7.
49. Sobue G. The role of Schwann cells in peripheral nerve degeneration and regeneration—NGF-NGF receptor system. *Rinsho shinkeigaku = Clinical neurology*. 1990;30(12):1358-60.
50. Gambarotta G, Fregnan F, Gnani S, Perroteau I. Neuregulin 1 role in Schwann cell regulation and potential applications to promote peripheral nerve regeneration. *Tissue Engineering of the Peripheral Nerve: Stem Cells and Regeneration Promoting Factors*. 2013;108:223-256. doi: 10.1016/B978-0-12-410499-0.00009-5.
51. Tonda-Turo C, Ruini F, Gnani S, et al. Naturally-derived hydrogels for growth factors release in peripheral nerve tissue engineering. *J. Tiss. Eng. Regen. Med*. 2012;6:79-79.
52. Scholz T, Rogers JM, Krichevsky A, Dhar S, Evans GRD. Inducible nerve growth factor delivery for peripheral nerve regeneration *in vivo*. *Plast. Reconstr. Surg*. 2010;126(6):1874-1889. doi: 10.1097/PRS.0b013e3181f5274e.
53. Wood MD, Hunter D, Mackinnon SE, Sakiyama-Elbert SE. Heparin-binding-affinity-based delivery systems releasing nerve growth factor enhance sciatic nerve regeneration. *J. Biomater. Sci. Polym. Ed*. 2010;2 1(6-7):77 1-787. doi: 10.1163/156856209X445285.
54. Kemp SWP, Webb AA, Midha R. Sensorimotor analysis of peripheral nerve regeneration through T-tube chambers loaded with nerve growth factor (NGF). *J. Peripheral Nervous System*. 2009;14:73-74.
55. Valmikinathan CM, Defroda S, Yu X. Polycaprolactone and bovine serum albumin based nanofibers for controlled release of nerve growth factor. *Biomacromolecules*. 2009;10(5):1084-1089. doi: 10.1021/bm8012499.
56. Yu H, Peng J, Guo Q, et al. Improvement of peripheral nerve regeneration in acellular nerve grafts with local release of nerve growth factor. *Microsurgery*. 2009;29(4):330-336. doi: 10.1002/micr.20635.
57. de Boer R, Knight AM, Wang H, et al. Microsphere delivery of nerve growth factor (NGF) and glial cell line derived neurotrophic factor (GDNF) in supporting peripheral nerve regeneration in polymer scaffolds. *Ann. Neurol*. 2008;64:S31-S32.

58. Kemp SWP, Walsh SK, Midha R. Growth factor and stem cell enhanced conduits in peripheral nerve regeneration and repair. *Neurol. Res.* 2008;30(10): 1030-1038. doi: 10.1179/174313208X362505.
59. Lee AC, Yu VM, Lowe JB, et al. Controlled release of nerve growth factor enhances sciatic nerve regeneration. *Exp. Neurol.* 2003;184(1):295-303. doi: 10.1016/S0014-4886(03)00258-9.
60. Aizawa H, Ugawa Y, Genba K, Shimpo T, Mannen T. [Percutaneous electrical stimulation (PES) and SEP in peripheral neuropathies]. *Rinsho shinkeigaku = Clinical neurology.* 1988;28(4):447-52.
61. Xu XY, Yee WC, Hwang PYK, et al. Peripheral nerve regeneration with sustained release of poly(phosphoester) microencapsulated nerve growth factor within nerve guide conduits. *Biomaterials.* 2003;24(13):2405-2412. doi: 10.1016/S0142-9612(03)00109-1.
62. Heine J, Schmiedl A, Cebotari S, et al. Preclinical assessment of a tissue-engineered vasomotive human small-calibered vessel based on a decellularized xenogenic matrix: Histological and functional characterization. *Tiss. Eng. Part A.* 2011;17(9-10): 1253-1261. doi: 10.1089/ten.tea.2010.0375.
63. McCallister WV, Tang P, Smith J, Trumble TE. Axonal regeneration stimulated by the combination of nerve growth factor and ciliary neurotrophic factor in an end-to-side model. *J. Hand Surg.* 2001;26A(3):478-488. doi: 10.1053/jhsu.2001.24148.
64. Brown MC, Perry VH, Lunn ER, Gordon S, Heumann R. Macrophage dependence of peripheral sensory nerve regeneration - possible involvement of nerve growth-factor. *Neuron.* 1991;6(3):359-370. doi: 10.1016/0896-6273(91)90245-U.
65. Lee JY, Bashur CA, Goldstein AS, Schmidt CE. Polypyrrole-coated electrospun PLGA nanofibers for neural tissue applications. *Biomaterials.* 2009;30(26):4325-4335. doi: 10.1016/j.biomaterials.2009.04.042.
66. Jiang XP, Tessier D, Dao LH, Zhang Z. Biostability of electrically conductive polyester fabrics: An *in vitro* study. *J. Biomed. Mater. Res.* 2002;62(4):507-513. doi: 10.1002/jbm.10240.
67. Zawko SA, Schmidt CE. Simple benchtop patterning of hydrogel grids for living cell microarrays. *Lab Chip.* 2010;10(3):379-383. doi: 10.1039/b917493a.

68. Fonner JM, Forciniti L, Nguyen H, et al. Biocompatibility implications of polypyrrole synthesis techniques. *Biomed. Mater.* 2008;3(3):034124. doi: 10.1088/1748-6041/3/3/034124.
69. Gordon T, Udina E, Verge VMK, de Chaves EIP. Brief electrical stimulation accelerates axon regeneration in the peripheral nervous system and promotes sensory axon regeneration in the central nervous system (vol 13, pg 412, 2009). *Motor Control.* 2010;14(1):147-147.
70. Gordon T, Udina E, Verge VMK, de Chaves EIP. Brief electrical stimulation accelerates axon regeneration in the peripheral nervous system and promotes sensory axon regeneration in the central nervous system. *Motor Control.* 2009;13(4):412-441.
71. Al-Majed AA, Neumann CM, Brushart TM, Gordon T. Brief electrical stimulation promotes the speed and accuracy of motor axonal regeneration. *J. Neurosci.* 2000;20(7):2602-2608.
72. Brooks DN, Weber RV, Chao JD, et al. Processed nerve allografts for peripheral nerve reconstruction: A multicenter study of utilization and outcomes in sensory, mixed, and motor nerve reconstructions. *Microsurgery.* 2012;32(1): 1-14. doi: 10.1002/micr.20975.
73. Bechara S, Wadman L, Popat KC. Electroconductive polymeric nanowire templates facilitates *in vitro* C17.2 neural stem cell line adhesion, proliferation and differentiation. *Acta Biomaterialia.* 2011;7(7):2892-2901. doi: 10.1016/j.actbio.2011.04.009.
74. Moroder P, Runge MB, Wang H, et al. Material properties and electrical stimulation regimens of polycaprolactone fumarate-polypyrrole scaffolds as potential conductive nerve conduits. *Acta Biomater.* 2011;7(3):944-953. doi: 10.1016/j.actbio.2010.10.013.
75. Runge MB, Dadsetan M, Baltrusaitis J, et al. The development of electrically conductive polycaprolactone fumarate-polypyrrole composite materials for nerve regeneration. *Biomaterials.* 2010;31(23):5916-5926. doi: 10.1016/j.biomaterials.2010.04.012.
76. Runge MB, Dadsetan M, Baltrusaitis J, et al. Development of electrically conductive oligo(polyethylene glycol) fumarate-polypyrrole hydrogels for nerve regeneration. *Biomacromolecules.* 2010;11(11):2845-2853. doi: 10.1021/bml00526a.
77. Runge MB, Wang H, Spinner Rj, Windebank AJ, Yaszemski MJ. Reformulating polycaprolactone fumarate to eliminate toxic diethylene glycol: Effects of polymeric branching and autoclave sterilization on material properties. *Acta Biomater.* 2012;8(1):133-143. doi: 10.1016/j.actbio.2011.08.023.

78. Eisazadeh H. Studying the characteristics of polypyrrole and its composites. *World J. Chem.* 2007;2(2):67-74.
79. Bruno FF, Fossey SA, Nagarajan S, Nagarajan R, Kumar J, Samuelson LA. Biomimetic synthesis of water-soluble conducting copolymers/homopolymers of pyrrole and 3,4-ethylenedioxythiophene. *Biomacromolecules.* 2006;7(2):586-589.
80. Hardy JG, Mouser DJ, Arroyo-Curras N, et al. Biodegradable electroactive polymers for electrochemically -triggered drug delivery. *Journal of Materials Chemistry B.* 2014;2, 6809-6822.
81. Bilston LE. Neural tissue biomechanics. Springer: Randwick, Australia, 2011; Vol. 3. doi: 10.1007/978-3-642-13890-4.
82. Guimard NKE, Sessler JL, Schmidt CE. Toward a biocompatible and biodegradable copolymer incorporating electroactive oligothiophene units. *Macromolecules.* 2009;42(2):502-511. doi: 10.1021/ma8019859.
83. da Silva MA, Crawford A, Mundy J, et al. Evaluation of extracellular matrix formation in polycaprolactone and starch-compounded polycaprolactone nanofiber meshes when seeded with bovine articular chondrocytes. *Tissue Eng. Part A.* 2009;15(2):377-385. doi: 10.1089/ten.tea.2007.0327.
84. Jukola H, Nikkola L, Gomes ME, et al. Development of a bioactive glass fiber reinforced starch-polycaprolactone composite. *J. Biomed. Mater. Res. Part B.* 2008;87B(1): 197-203. doi: 10.1002/jbm.b.31093.
85. Woodruff MA, Huttmacher DW. The return of a forgotten polymer-polycaprolactone in the 21st century. *Prog. Polym. Sci.* 2010;35(10): 1217-1256. doi: 10.1016/j.progpolymsci.2010.04.002.
86. Schmidt CE, Shastri VR, Vacanti JP, Langer R. Stimulation of neurite outgrowth using an electrically conducting polymer. *PNAS.* 1997;94(17):8948-8953. doi: 10.1073/pnas.94.17.8948.
87. Wang ZX, Roberge C, Dao LH, et al. *In vivo* evaluation of a novel electrically conductive polypyrrole/poly(D,L-lactide) composite and polypyrrole-coated-poly(D,L-lactide-co-glycolide) membranes. *J. Biomed. Mater. Res. Part A.* 2004;70A(1):28-38. doi: 10.1002/jbm.a.30047.
88. Mihardja SS, Sievers RE, Lee RJ. The effect of polypyrrole on arteriogenesis in an acute rat infarct model. *Biomaterials.* 2008;29(31):4205-4210. doi: 10.1016/j.biomaterials.2008.07.021.

89. Durgam H, Sapp S, Deister C, et al. Novel degradable co-polymers of polypyrrole support cell proliferation and enhance neurite out-growth with electrical stimulation. *J. Biomater. Sci. Polym. Ed.* 2010;2 1(10): 1265-1282. doi: 10.1163/092050609X12481751806330.
90. George PM, Lyckman AW, LaVan DA, et al. Fabrication and biocompatibility of polypyrrole implants suitable for neural prosthetics. *Biomaterials*. 2005;26(17):3511-3519. doi: 10.1016/j.biomaterials.2004.09.037.
91. Huang J, Ye Z, Hu X, Lu L, Luo Z. Electrical stimulation induces calcium-dependent release of NGF from cultured Schwann cells. *Glia*. 2010;58:622-631. doi: 10.1002/glia.20951.
92. Huang J, Hu X, Lu L, Ye Z, Zhang Q, Luo Z. Electrical regulation of Schwann cells using conductive polypyrrole/chitosan polymers. *J. Biomed. Mater. Res. Part A*. 2010;93A:164-174. doi: 10-1002/jbm.a.32511.
93. Zhu B, Luo SC, Zhao H, Lin HA, Sekine J, Nakao A, Chen C, Yamashita Y, Yu H. Large enhancement in neurite outgrowth on a cell membrane-mimicking conducting polymer. *Nat. Commun.* 2014;5:4523. doi: 10.1038/ncomms5523.
94. Koppes AN, Nordberg AL, Paolillo GM, et al. Electrical stimulation of Schwann cells promotes sustained increases in neurite outgrowth. *Tissue Eng. Part A*. 2014;20(3 and 4):494-506. doi: 10.1089/ten.tea.2013.0012.
95. George PM, LaVan DA, Burdick JA, Chen CY, Liang E, Langer R. Electrically controlled drug delivery from biotin-doped conductive polypyrrole. *Adv. Mater.* 2006;18(5):577-581. doi: 10.1002/adma.200501242.
96. Cho Y, Shi R, Ivanisevic A, Ben Borgens R. A mesoporous silica nanosphere-based drug delivery system using an electrically conducting polymer. *Nanotechnology*. 2009;20(27):275102. doi: 10.1088/0957-4484/20/27/275102
97. Liu J, Lamb D, Chou MM, Liu Y, Li G. Nerve growth factor-mediated neurite outgrowth via regulation of Rab5. *Mol Biol Cell*. 2007;18(4): 1375-1384. doi: 10.1091/mbc.E06-08-0725.
98. Hu ZQ, Ulfendahl M, Olivius NP. NGF stimulates extensive neurite outgrowth from implanted dorsal root ganglion neurons following transplantation into the adult rat inner ear. *Neurobiol Dis*. 2005;18(1):184-192. doi: 10.1016/j.nbd.2004.09.010.

It should be noted that ratios, concentrations, amounts, and other numerical data may be expressed herein in a range format. It is to be understood that such a range format is used

for convenience and brevity, and thus, should be interpreted in a flexible manner to include not only the numerical values explicitly recited as the limits of the range, but also to include all the individual numerical values or sub-ranges encompassed within that range as if each numerical value and sub-range is explicitly recited. To illustrate, a concentration range of "about 0.1% to about 5%" should be interpreted to include not only the explicitly recited concentration of about 0.1 wt% to about 5 wt%, but also include individual concentrations (*e.g.*, 1%, 2%, 3%, and 4%) and the sub-ranges (*e.g.*, 0.5%, 1.1%, 2.2%, 3.3%, and 4.4%) within the indicated range. In an embodiment, the term "about" can include traditional rounding according to significant figures of the numerical value. In addition, the phrase "about 'x' to 'y'" includes "about 'x' to about 'y'\"

Many variations and modifications may be made to the above-described embodiments. All such modifications and variations are intended to be included herein within the scope of this disclosure and protected by the following claims.

CLAIMS

We claim:

1. A method of forming a tissue scaffold, comprising:
mixing a solution including urea and a non-aqueous solvent with a polymer that is soluble with the solvent to form a mixture;
disposing the mixture on a substrate; and
removing the solvent from the mixture to form a tissue scaffold.
2. The method of claim 1, further comprising: removing the urea from the tissue scaffold to form a biodegradable porous tissue scaffold, wherein removal of the urea forms pores within the tissue scaffold to form the biodegradable porous tissue scaffold.
3. The method of claim 1, wherein the non-aqueous solvent is selected from the group consisting of: formic acid, trifluoroacetic acid, hexafluoroisopropanol, hexafluoroacetone hydrate, methanol, ethanol, propanol, isopropanol, acetophenone, methoxyethanol, ethanediol, 1,2-propanediol, 1,3-propanediol, glycerol, glycerol monoacetate, glycerol diacetate, methylacetate, ethylacetate, allyl alcohol, furfuryl alcohol, diacetone alcohol, benzyl alcohol, cyclohexanol and a combination thereof.
4. The method of claim 1, wherein the polymer is insoluble in water.
5. The method of claim 4, wherein the polymer is selected from the group consisting of: nylon, hydroxybutyric acids, polyanhydrides, polphosphazenes, polyphosphoesters, polyethers, polysilanes, polysiloxanes, polyurethanes,) polycaprolactone, polyesters, polyamides, PCL, PLLA, PLGA, lignins, polyalanine, oligoalanine, collagen, silk, cellulose, chitin, chitosan, dextran, and a combination thereof.
6. The method of claim 1, further comprising an electroactive tissue scaffold by polymerizing an electroactive polymer with the tissue scaffold.
7. The method of claim 6, further comprising: removing the urea from the electroactive tissue scaffold to form a biodegradable electroactive porous tissue scaffold, wherein removal

of the urea forms pores within the tissue scaffold to form the biodegradable electroactive porous tissue scaffold.

8. The method of claim 6, wherein the electroactive polymer is selected from the group consisting of: polypyrrole, polyaniline, polythiophene, poly(3,4-ethylenedioxythiophene), poly fluorenes, polyphenylenes, polypyrenes, polyazulenes, polynaphthalenes, polyindoles, polyazepines, poly(p-phenylene sulfide)s, poly(p-phenylene vinylene)s, polyfurans, and a combination thereof.

9. The method of claim 1, wherein the substrate includes a network of channels, wherein the mixture is disposed in the network of channels, wherein further comprising: removing the substrate to form the tissue scaffold having a network of pores extending through the tissue scaffold.

10. The method of claim 9, wherein the network of channels are aligned relative to one another and each of the channels in the network of channels has a diameter of about 50 nm to 100 μm and the length of about 1 cm to 10 cm.

11. The method of claim 9, further comprising: removing the urea from the tissue scaffold to form a biodegradable porous tissue scaffold, wherein removal of the urea forms pores within the tissue scaffold to form the biodegradable porous tissue scaffold.

12. The method of claim 11, wherein the pores formed from removal of the urea are of the type selected from the group consisting of: dendritic, linear, and a combination thereof.

13. A structure, comprising:
a tissue scaffold including a polymer and urea, wherein the polymer is soluble in a non-aqueous solvent selected from the group consisting of: formic acid, trifluoroacetic acid, hexafluoroisopropanol, hexafluoroacetone hydrate, methanol, ethanol, propanol, isopropanol, acetophenone, methoxyethanol, ethanediol, 1,2-propanediol, 1,3-propanediol, glycerol, glycerol monoacetate, glycerol diacetate, methylacetate, ethylacetate, allyl alcohol, furfuryl alcohol, diacetone alcohol, benzyl alcohol, cyclohexanol and a combination thereof.

14. The structure of claim 13, wherein the polymer is not soluble in water.

15. The structure of claim 14, wherein the polymer is selected from the group consisting of: nylon, hydroxybutyric acids, polyanhydrides, polphosphazenes, polyphosphoesters, polyethers, polysilanes, polysiloxanes, polyurethanes, polycaprolactone, polyesters, polyamides, PCL, PLLA, PLGA, lignins, polyalanine, oligoalanine, collagen, silk, cellulose, chitin, chitosan, dextran, and a combination thereof.
16. The structure of claim 13, further comprising an electroactive polymer.
17. The structure of claim 16, wherein the electroactive polymer is selected from the group consisting of: polypyrrole, polyaniline, polythiophene, poly(3,4-ethylenedioxythiophene), poly fluorenes, polyphenylenes, polypyrenes, polyazulenes, polynaphthalenes, polyindoles, polyazepines, poly(p-phenylene sulfide)s, poly(p-phenylene vinylene)s, polyfurans, and a combination thereof.
18. The structure of claim 13, wherein the urea is in the form of urea crystals, wherein the urea crystals have a crystal structure selected from the group consisting of: dendritic, linear, or a combination thereof.
19. The structure of claim 13, wherein the tissue scaffold includes a network of channels that are aligned relative to one another and each of the channels in the network of channels has a diameter of 50 nm to 100 μm and the length of about 1 cm to 10 cm.

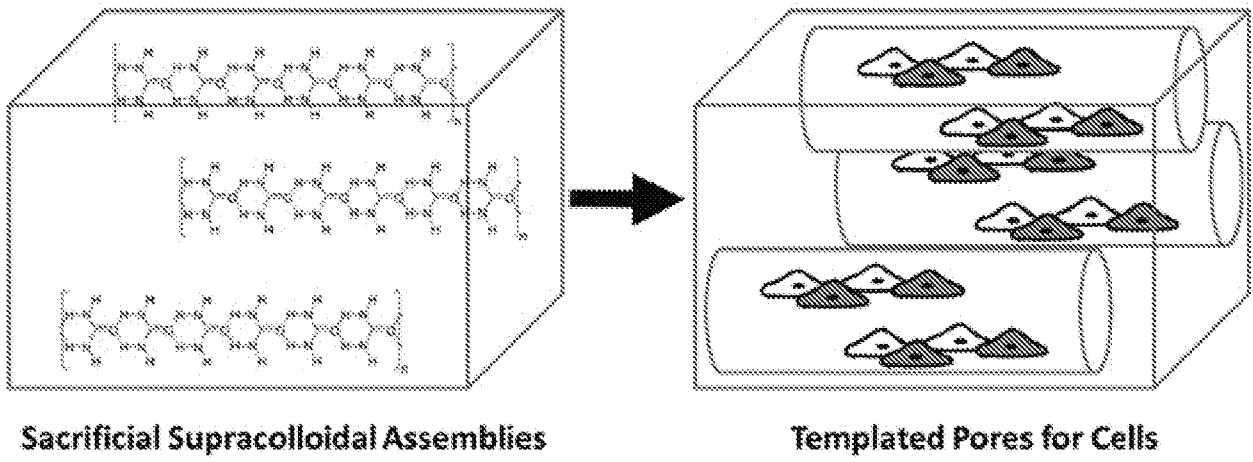


Fig. 1.1

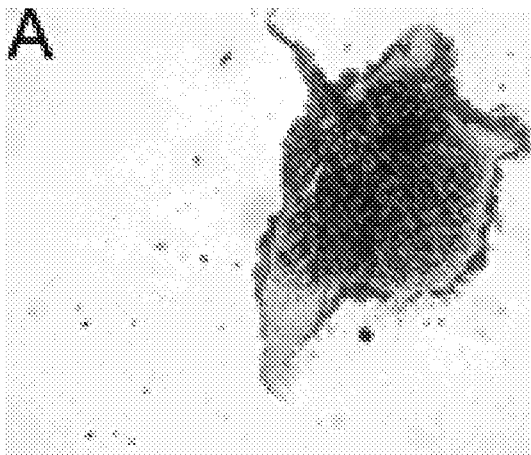


Fig. 1.2A



Fig. 1.2B

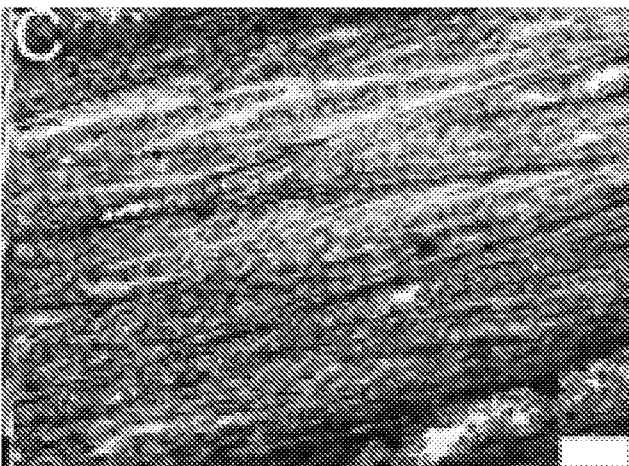


Fig. 1.2C

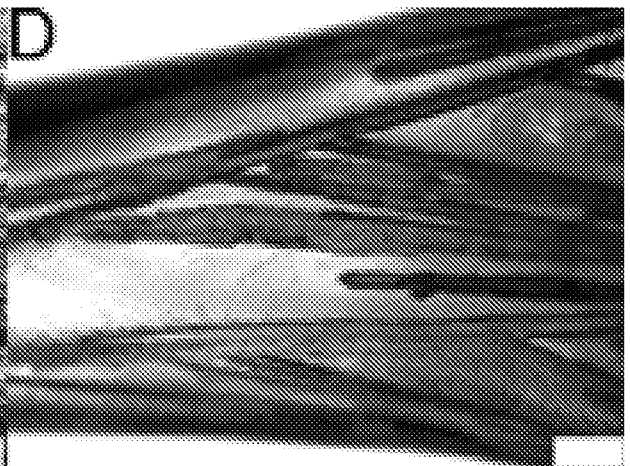


Fig. 1.2D

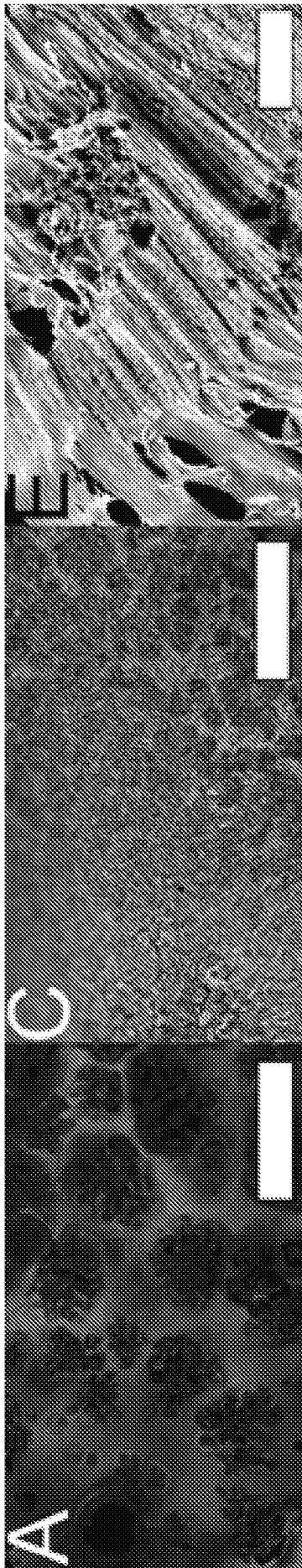


Fig. 1.3A

Fig. 1.3C

Fig. 1.3E

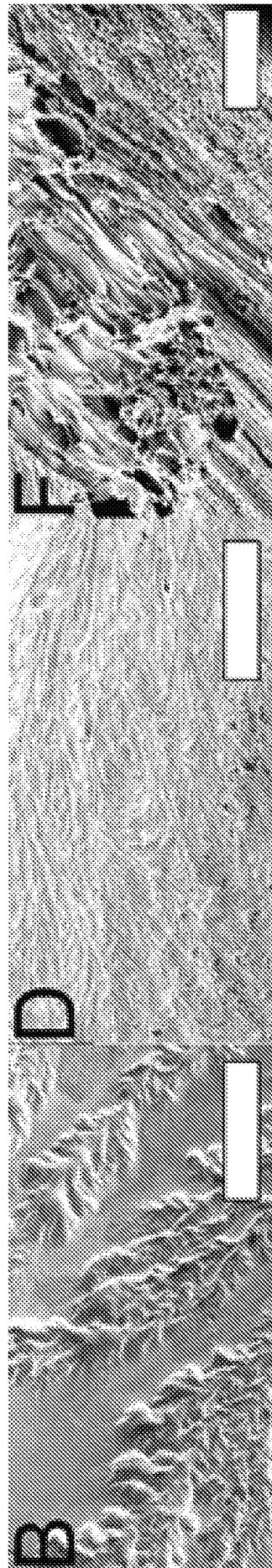


Fig. 1.3B

Fig. 1.3D

Fig. 1.3F

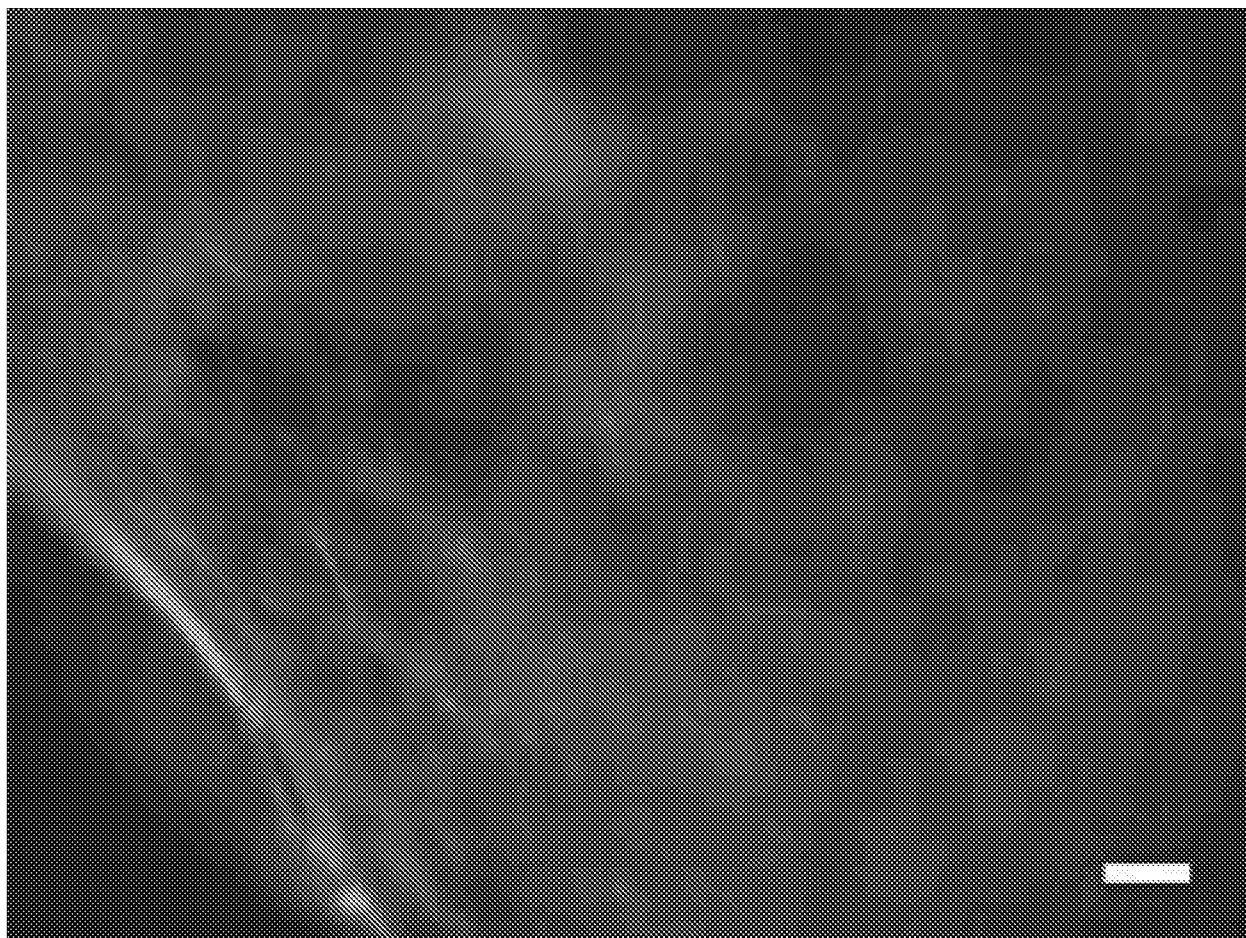


Fig. 1.4

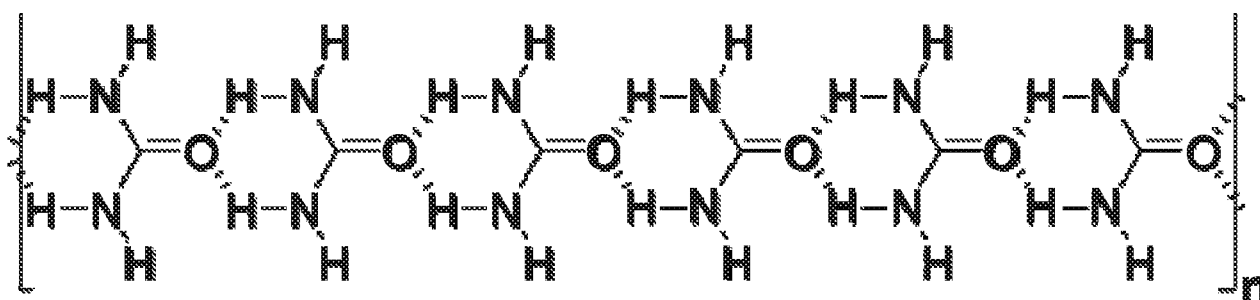


Fig. 2.1

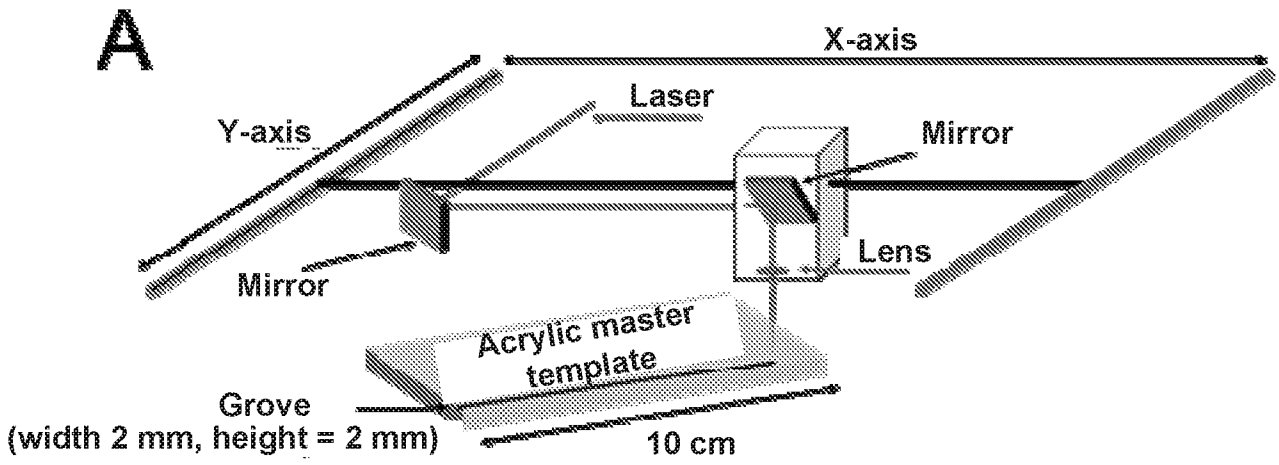


Fig. 2.2A

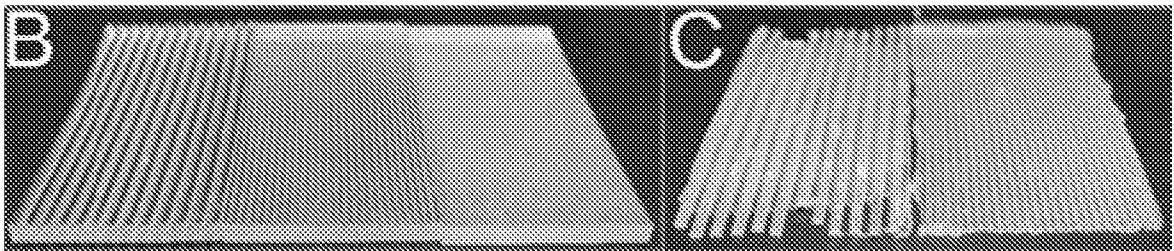


Fig. 2.2B

Fig. 2.2C

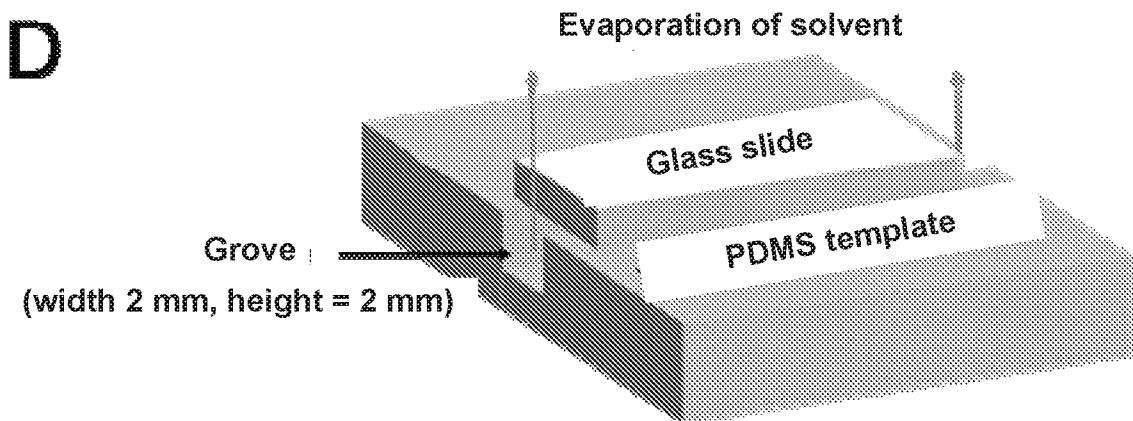


Fig. 2.2D

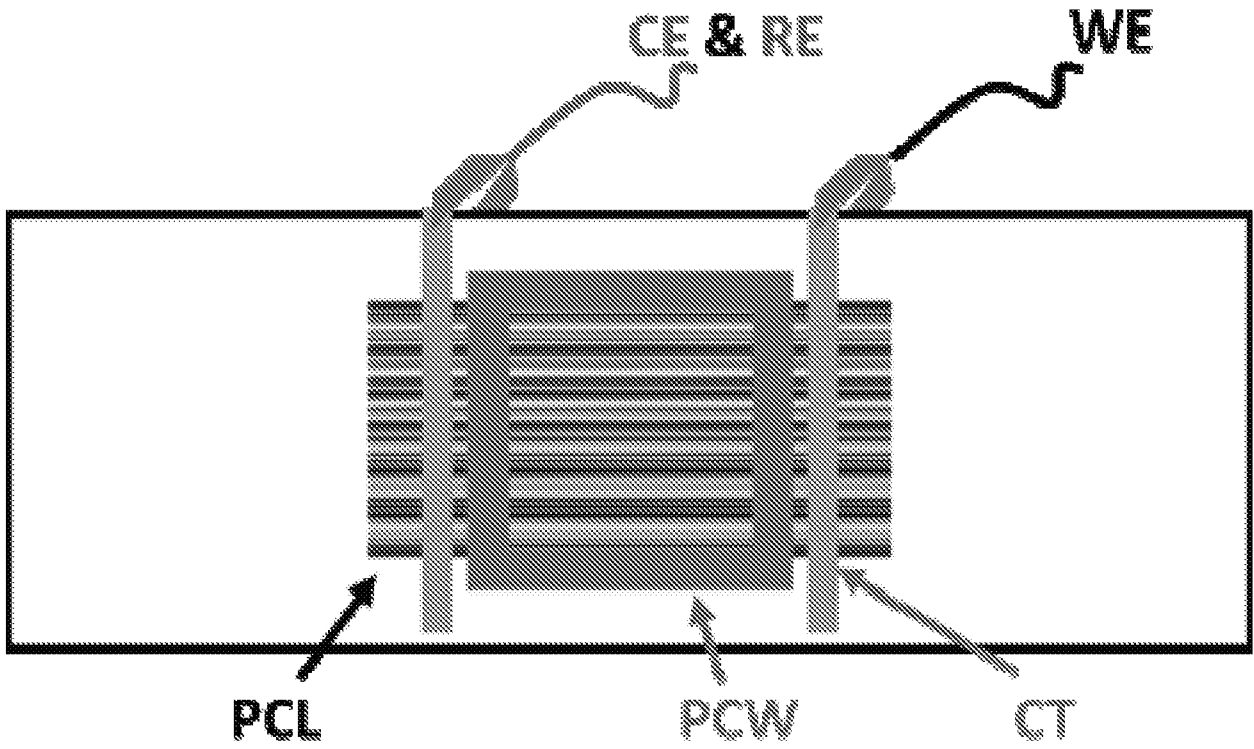


Fig. 2.3

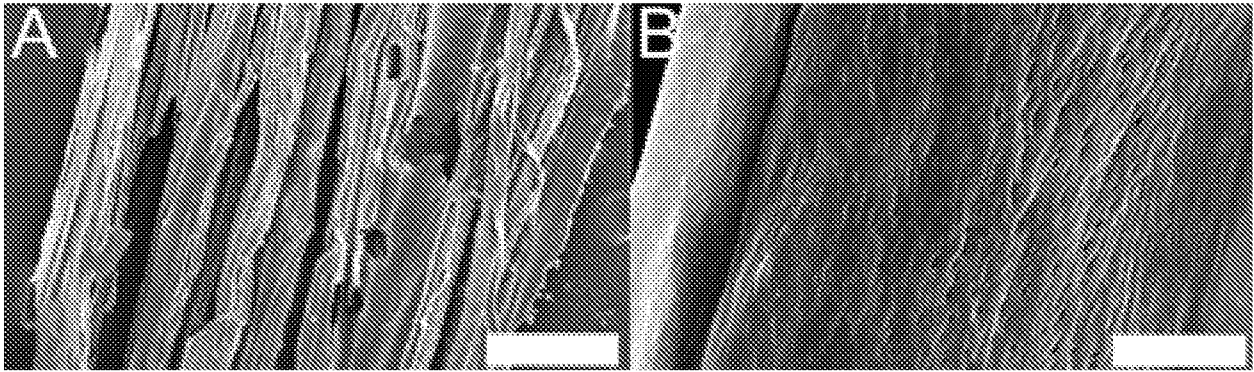


Fig. 2.4A

Fig. 2.4B

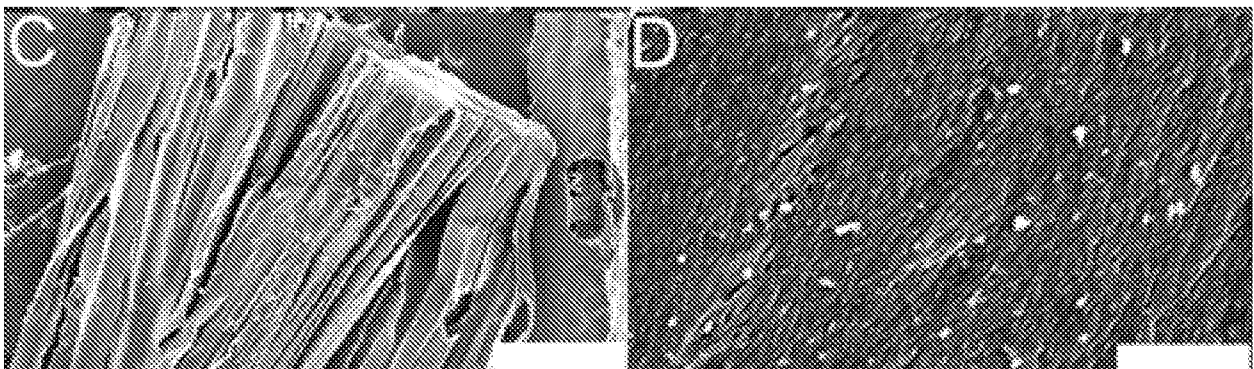


Fig. 2.4C

Fig. 2.4D

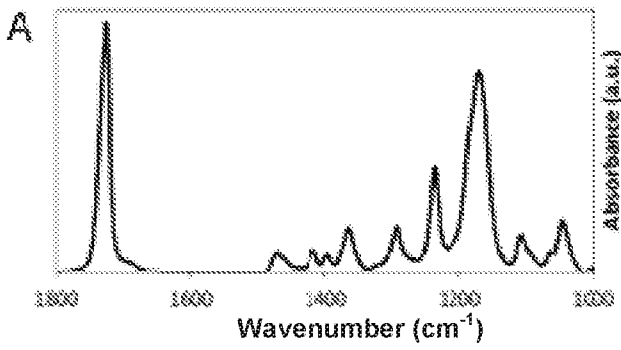


Fig. 2.5A

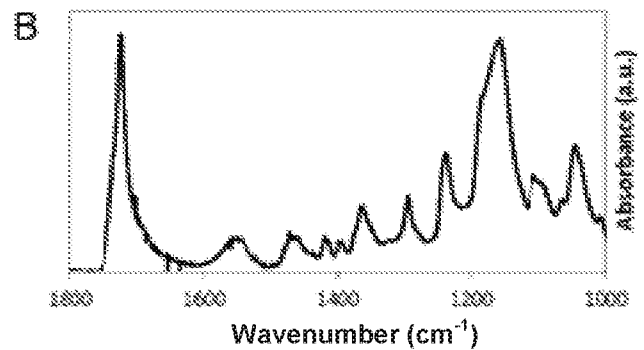


Fig. 2.5B

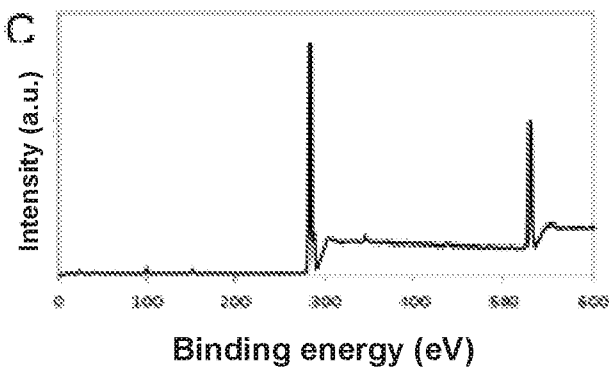


Fig. 2.5C

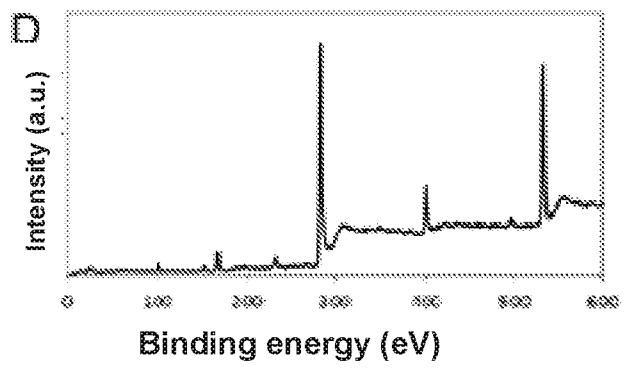


Fig. 2.5D

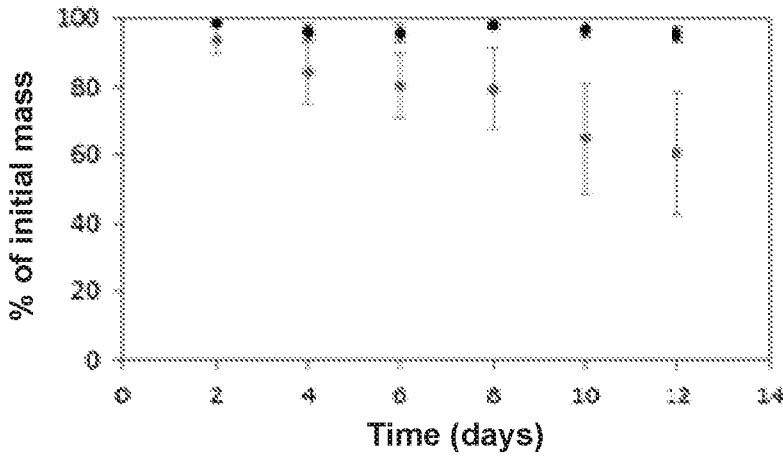
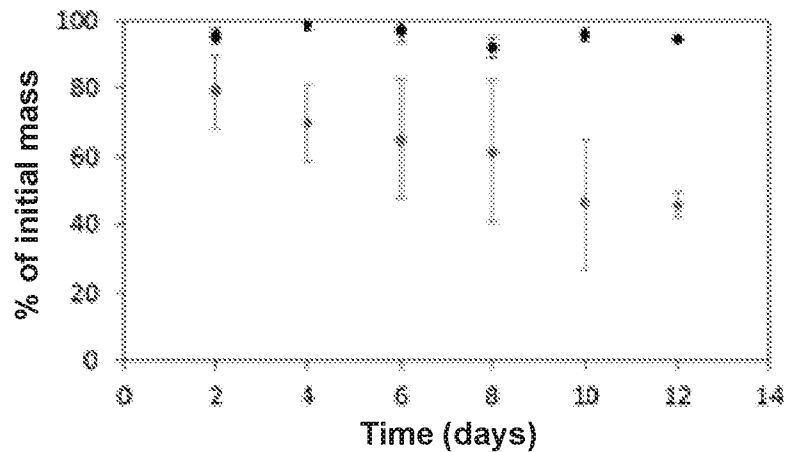


Fig. 2.6A

Fig. 2.6B



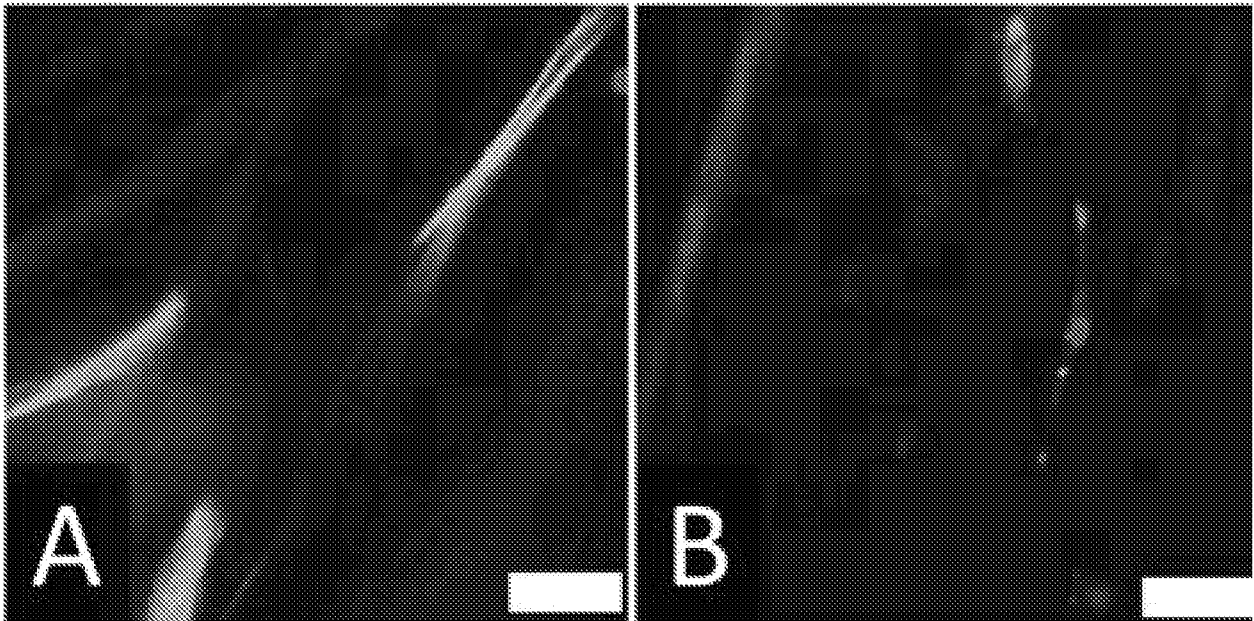


Fig. 2.7A

Fig. 2.7B

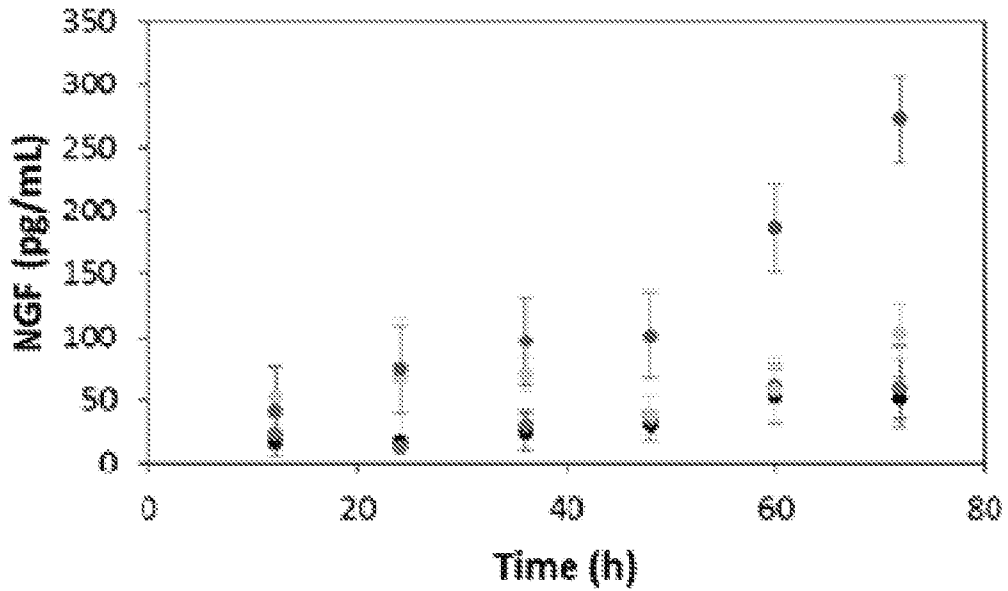


Fig. 2.8

INTERNATIONAL SEARCH REPORT

International application Hu.
PCT/US1 5/60329

A. CLASSIFICATION OF SUBJECT MATTER
 IPC(8) - A61F 2/02 (2015.01)
 CPC - A61F 2/02
 According to International Patent Classification (IPC) or to both national classification and IPC

B. FIELDS SEARCHED
 Minimum documentation searched (classification system followed by classification symbols)
 IPC(8): A61F 2/02, 2/06; A61L 27/56 (2015.01)
 CPC: A61 F 2/02, 2002/30766; A61L 27/56

Documentation searched other than minimum documentation to the extent that such documents are included in the fields searched

Electronic data base consulted during the international search (name of data base and, where practicable, search terms used)
 PatSeer (US, EP, WO, JP, DE, GB, CN, FR, KR, ES, AU, IN, CA, INPADOC Data) EBSCO; IEEE.com; Google Scholar, Google Patent; tissue scaffold, urea, carbamide, diamine, solvent, polymer, electroactive, substrate, mold, mixing, composition, evaporation, pores, channel, network, removal, separation.

C. DOCUMENTS CONSIDERED TO BE RELEVANT

Category*	Citation of document, with indication, where appropriate, of the relevant passages	Relevant to claim No.
X	KR 10076051 1 B 1 (KOREA INST SCI & TECH) 04 October 2007; claims 1, 8; paragraphs [0008], [0012]-[0013], [0019], [0021], [0036], [0069]	1-5, 13-15
Y		6-12, 16-19
Y	US 2013/0131830 A 1 (LELKES, P I et al.) 23 May 2013; abstract, paragraphs [0009]-[0010], [0051]-[0052]	6-8, 16-17
Y	US 201 1/0129515 A 1 (ARCHIBALD, SJ) 02 June 201 1; paragraphs [0028], [0034]	10, 12, 18-19
Y	US 2014/0081384 A 1 (HOGANSON, DM) 20 March 2014; paragraphs [0009], [0058], [0063], [0065]	9-12
A	US 2014/0099277 A 1 (POLYNOVO BIOMATERIALS PTY LIMITED) 10 April 2014; entire document	1-19
A	WO 2013/095138 A 1 (POLYGANICS B.V.) 27 June 2013; entire document	1-19
A	US 2006/0069435 A 1 (BROWN, KR et al.) 30 March 2006; entire document	1-19

Further documents are listed in the continuation of Box C. See patent family annex.

* Special categories of cited documents:
 "A" document defining the general state of the art which is not considered to be of particular relevance
 "E" earlier application or patent but published on or after the international filing date
 "L" document which may throw doubts on priority claim(s) or which is cited to establish the publication date of another citation or other special reason (as specified)
 "O" document referring to an oral disclosure, use, exhibition or other means
 "P" document published prior to the international filing date but later than the priority date claimed
 "T" later document published after the international filing date or priority date and not in conflict with the application but cited to understand the principle or theory underlying the invention
 "X" document of particular relevance; the claimed invention cannot be considered novel or cannot be considered to involve an inventive step when the document is taken alone
 "Y" document of particular relevance; the claimed invention cannot be considered to involve an inventive step when the document is combined with one or more other such documents, such combination being obvious to a person skilled in the art
 "&" document member of the same patent family

Date of the actual completion of the international search: 23 December 2015 (23.12.2015)
 Date of mailing of the international search report: **02 FEB 2016**

Name and mailing address of the ISA/
 Mail Stop PCT, Attn: ISA/US, Commissioner for Patents
 P.O. Box 1450, Alexandria, Virginia 22313-1450
 Facsimile No. 571-273-8300
 Authorized officer: Shane Thomas
 PCT Helpdesk: 571-272-4300
 PCT OSP: 571-272-7774